PNAS
www.pnas.org

Supplementary Information for

Ongoing Global and Regional Adaptive Evolution of SARS-CoV-2

Nash D. Rochman, Yuri I. Wolf, Guilhem Faure, Pascal Mutz, Feng Zhang, and Eugene V. Koonin

Nash D. Rochman
Email: nash.rochman@nih.gov

Feng Zhang
Email: zhang@broadinstitute.org

Eugene V. Koonin
Email: koonin@ncbi.nlm.nih.gov

This PDF file includes:

Detailed Methods
Figures S1 to S25
Tables S1 to S5

Additional supplementary information can be found at this address:

https://ftp.ncbi.nih.gov/pub/wolf/_suppl/SARSevo21/

This repository includes:

The global tree in Newick format: global_2_13_21.main.tre
The global, ultrametric tree in Newick format: global_2_13_21.ultra.tre
All metadata used in this study including the GISAID acknowledgements: metadata.tgz
Tables S1-S4 in plain text format.

Methods

Multiple alignment of SARS-CoV-2 genomes

All SARS-CoV-2 genomes that were available as of January 8, 2021 were retrieved from the Gisaid(1) database, which at that time comprised the vast majority of available sequences. Earlier iterations of this protocol had been previously completed from all available sequences including Genbank(2) and CNCB(3) as well. Sequences with apparent anomalies (sequence inversion etc.) were immediately discarded. Sequences were harmonized to DNA (e.g. U was transformed to T to amend software compatibility) and clustered according to 100% identity with no coverage threshold using CD-HIT(4, 5), with ambiguous characters masked. All characters excepting ACGT were considered ambiguous. The least ambiguous sequence from each cluster was selected and sequences shorter than 25120 nucleotides were discarded.

Exterior ambiguous characters (preceding/succeeding the first/last defined nucleotide) were removed, and sequences with more than 10 remaining interior, ambiguous characters were discarded. A reference alignment was previously constructed using the same protocol as follows with the exception of the --keeplength specification in November, 2020. The updated database was aligned using multi-threaded MAFFT(6) with 80 cores (--thread 80, when more cores were allocated they were not utilized) and 3.8Tb of RAM to maintain usage of the normal DP algorithm(6) (--nomemsave) against this reference alignment (specifying --keeplength). Aligning “from scratch” without --keeplength proved to be prohibitively slow so we recommend first constructing a reference alignment from a suitable subset of sequences. Sequences sourced from non-human hosts were manually identified from the metadata and those excluded at the previous step were added to the alignment using MAFFT, (again specifying --keeplength). Note that use of the --keeplength option will not include insertions relative to the reference alignment.

Sites corresponding to protein-coding ORFs were then mapped to the alignment from the reference sequence NC_045512.2 excluding stop codons as follows: 266-13468+13468-21552, orf1ab; 21563-25381, S; 25393-26217, orf3a; 26245-26469, E; 26523-27188, M; 27202-27384, orf6; 27394-27756, orf7a; 27756-27884, orf7b; 27894-28256, orf8; and 28274-29530, N. The remaining sites were discarded.

The resulting alignment contained out-of-frame gaps. Gaps in the reference sequence, corresponding to insertions, were found to correspond to gaps in all but fewer than 1% of the remaining sequences (all gaps in the reference sequence correspond to gaps in the alignment from November, 2020, the use of --keeplength prohibited the recognition of any insertions relative to the reference sequence which were not present in this reference alignment). These sites were discarded. The remaining gaps, corresponding to deletions relative to the reference sequence, shorter than three nucleotides were replaced with the ambiguous character, N. Longer gaps were shifted into frame and padded with ambiguous characters on either end of the gap, minimizing the number of sites altered.

A fast, approximate tree was then built using FastTree(7) (parameters: -nt -gtr -gamma -nosupport -fastest) to unambiguously define two clusters of sequences: an outgroup consisting of 14 sequences sourced from non-human hosts prior to 2020 and the main group. The tree construction requires the resolution of very short branch lengths which makes it necessary to compile FastTree at double precision. Outliers from the remaining sequences were then identified based on the Hamming distance (excluding gaps and ambiguous characters) to the nearest neighbor, the Hamming distance to the consensus, and the degree to which those substitutions relative to consensus were clustered in the genome. At this step, 81 sequences were removed.

The resulting alignment, consisting of 98,090 sequences and 29,119 sites, was maintained for the construction of the global tree and ancestral sequence reconstruction. In an effort to minimize the impact of sequencing error on the tree topology, as well as to decrease computational costs, a reduced alignment was then constructed through the removal of 1) invariant sites, 2) sites invariant with the exception of a single sequence, and 3) sites invariant throughout the main group with the exception of at most one sequence representing each minority nucleotide. Removing these sites created substantial redundancy, so a representative sequence was selected for each cluster of 100% identity to yield an alignment consisting of 90,585 sequences and 16,487 sites. As described below and in the main text, a third alignment was constructed including only the top 5% of sites with the most common substitutions relative to consensus (of this second alignment) and again removing redundant sequences to yield 32,563 sequences and 834 sites.

Tree Construction

We sought to optimize tree topology with IQ-TREE(8); however, building the global tree was computationally prohibitive, and thus, we proceeded to subsample the smallest alignment (834 sites) as follows. First, a core set of maximally diverse sequences is selected. The set is initialized with a pair of sequences: a sequence maximizing the number of substitutions relative to consensus and a paired sequence which maximizes the Hamming distance to itself. Sequences are then added to this core set one at a time maximizing the minimum Hamming distance to any representative of the set until *N* sequences are incorporated. Next, $ceil\left(L/(M-N)\right)$ resulting sets are initialized with this core set where *M* is the target number of sequences and *L* is the total number of sequences in the alignment (32,363). Then, sequences that have not yet been incorporated into any resulting set are added to each resulting set, again one at a time, maximizing the minimum distance to any representative of the set until *M* sequences are incorporated. The order of the resulting sets is randomized at each iteration without repeats. Once every (main group) sequence has been incorporated into at least one resulting set, sequences are randomly incorporated into each set until every set contains *M* sequences. Finally, the outgroup is added to each resulting set. We chose *M*=3,000 in an effort to optimize computational efficiency and *N*=300.

Note that while increasing *N* increases the number of sets required for alignment coverage, and thus compute time, insufficient overlap between the sequences assigned each sub-alignment greatly affects the results of subsequent steps. As discussed in the main text, executing this protocol on an alignment containing most or all sites may not yield a consistent deep tree topology or “skeleton” since maximizing the hamming distance of any subset over all sites does not guarantee maximizing the tree distance in the resultant global topology. This is why limiting the alignment to sites with common substitutions relative to consensus is essential at this step.

A tree was then built, using IQ-TREE, for each maximally diverse set, with the evolutionary model fixed to GTR+F+G4 and the minimum branch length decreased from the default 10e-6 to 10e-7, according to the results of previous parameter studies(9). These trees were then converted into constraint files and merged to generate a single global constraint file for use within FastTree (parameters: -nt -gtr -gamma -cat 4 -nosupport -constraints).
The remaining sequences excluded from this tree but present in the second alignment (90,585 sequences and 16,487 sites) were then reintroduced as unresolved multifurcations and a new constraint file from the multifurcated tree was constructed. A second iteration of FastTree was initiated on the second alignment to produce an intermediate tree. This tree was primarily constructed as an intermediate step to limit the impact of sequencing errors on the final topology as mentioned in the main text; however, it is also less computationally intensive. The last step was then repeated on this intermediate tree to construct the global topology for the whole alignment. The final, global tree was rooted at the outgroup.

Reconstruction of Ancestral Genome Sequences

Ancestral states were estimated by Fitch Traceback(10). Briefly, character sets were constructed from leaf to root where each node was assigned the intersection of the descendant character sets if not empty and the union otherwise. Then, moving from root to leaf, nodes with more than one character in their set were assigned the consensus character if present in their set or a randomly chosen representative character otherwise. Substitutions between states were identified and placed in the middle of the branch bridging the pair of nodes.

Statistical associations between mutations were computed in a manner similar to that previously described(11). Briefly, sequences were leaf-weighted based on the branch lengths of the ultrameterized, tree. Every mutation present across the tree at 200 mean leaf-weight equivalents or more was considered. The probability of independent co-occurrence between any pair was estimated in two ways. An arbitrary member of the pair was selected as the ancestral mutation, and the binomial probability:

$$\sum_{k=N_{pair}}^{N_{total}} \binom{N_{total}}{k} F^k (1-F)^{N_{total}-k}$$

was computed where *N_total* is the number of substitutions to the descendant mutation across the entire ancestral record, *N_pair* is the number of substitutions to the descendant which succeed or appear simultaneously with a substitution to the ancestral mutation, and *F* is the fraction of the tree (fraction of all applicable branch lengths) occupied by the ancestral mutation. The ancestral/descendent designation was then reversed and the “binomial score” was constructed as the negative log of the product of these two terms. Additionally, for each pair, the observed and expected (product of the tree fractions) tree intersections were calculated and the “Poisson score” (analogous to the log-odds ratio) was calculated:

$$\begin{cases} -\ln\big(1-PCDF(exp,obs)\big), obs > exp \\ \ln\big(PCDF(exp,obs)\big), obs < exp \end{cases}$$

where PCDF(exp,obs) is the cumulative probability of a Poisson distribution with mean “exp”, the expected value of the data, and evaluated at “obs”, the observed value of the data. Both scores are reported. SI Appendix, Table S3 displays putative positively selected mutations with both scores above 5 or at least two simultaneous substitutions. Fig. 1D only displays associations between mutations in the N or S proteins. SI Appendix, Fig. S10 does not exclude mutations with NCN context but meets all other statistical criteria for positive selection and does not display mutations in the polyprotein.

Classical Multidimensional Scaling of the MSA

Pairwise Hamming distances were computed for all pairs of rows in the global MSA ignoring gaps and ambiguous characters i.e. the sequences *X*=”ATN-A” and *Y*=”NTAAT” would be assigned a distance of 1. The resulting distance matrix was embedded in three dimensions with the MATLAB(12) routine “cmdscale”. 100 rounds of stochastically initiated k-means clustering of the embedding was conducted and the optimum cluster number was determined to be 5 on the basis of the silhouette score distribution (SI Appendix, Fig S1). The silhouette score measures the similarity of each point to its own cluster relative to points in other clusters. For each point, it is defined as: min_over_clusters[(<d_other>-

<d_self>)/max(<d_other>,<d_self>)] where <d_other> is the mean distance from that value to values in a different cluster and <d_self> is the mean distance from that value to values in the same cluster. It ranges from -1 to 1.

Validation of Mutagenic Contexts

Mutations were divided into four categories: synonymous vs non-synonymous substitutions and high vs low frequency of independent occurrence. For example, consider codon X with 3 non-synonymous substitutions gat->ggt and 1 non-synonymous substitution gat->cgt. In this context, a non-synonymous nucleotide substitution a->g of frequency 4 would be recorded in nucleotide (X-1)*3+2. The low vs high frequency threshold was determined by the 90th percentile of the synonymous mutation frequency distribution (operationally 7). For each mutation, the trinucleotide contexts from the ancestral reconstruction at the nodes where the mutation occurred were compared to the background genome-wide frequencies, computed for the inferred common ancestor of SARS-CoV-2.

The expected frequencies of the trinucleotides using the background distribution were tabulated; the Yates correction (+/-0.5 to the original count depending on whether the count is below or above the expectation) was applied to the observed frequencies; the log-odds ratios of the (corrected) observed frequencies to the expectation were computed; and CMDS was applied to the Euclidean distances between the log-odds vectors to embed the points onto a plane (SI Appendix, Fig. S4 A.). This analysis was then repeated, this time, distinguishing only between high and low frequency substitutions but not N and S (SI Appendix, Fig. S4 B). Finally, the differences in the contexts of high frequency synonymous vs non-synonymous events were considered in the same manner and the chi-square statistics ((observed-expected)^2/expected) were compared with the critical chi-square value (p=0.05/64, df=1, SI Appendix, Fig. S4 C.).

Computation of *dN/dS*

For each of the 24 ORFs (splitting orf1ab into 15 segments corresponding to the 15 mature proteins, nsp11 and nsp12 combined), 10 reduced alignments were constructed as follows. Sequences were ordered based on diversity, in the same order with which they were included in the constraint trees. The first 10 sequences are conserved across every alignment and the remaining 40 are unique to each alignment. The reference sequence, NC_045512.2, was additionally added to each reduced alignment. PAML(13) was then used to estimate tN, tS, *dN/dS*, N, S, and N/S for each segment and every reduced alignment.

Given the global ancestral reconstruction from Fitch traceback, the total number of non-synonymous and synonymous substitutions (nN and nS, respectively) as well as these tallies normalized by the respective segment length (tN, and tS, respectively) were retrieved for each segment. A hybrid *dN/dS* value for each segment was estimated to be (nN/nS)/(N/S)* where (N/S)* is the median value of N/S across all repeats for the segment.

Metadata Assignment

Headers for all isolates belonging to CD-HIT clusters with a representative incorporated into the alignment with fewer than 10 interior ambiguous characters were processed to extract the sequencing date and location. Sequencing location abbreviations were matched to full names and the latitude/longitude of a representative city for each location was retrieved from simplemaps (https://simplemaps.com/data/world-cities)(14).

Regional Divergence Analysis

Two approaches, one partition dependent and one partition independent, were used as described in the main text. The Hellinger distance between regions over a sliding time window was computed between regions for the 11 (partitions/variant clades) group distribution. Next, 400 isolates were randomly selected from each region over a sliding window and 200 pairs within each region as well as 200 pairs between each pair of regions were composed. The tree distance between each pair was computed and the mean for each inter- and intra-regional pair tree-distance distribution was recorded. In Figs. 3C and S16, the 25th, 50th, and 75th percentiles are shown of the 15 possible pairs of (6) regions. Regions are selected based on GISAID metadata. The inter-regional tree divergence (Figs. 3C, top and SI Appendix, S16C) is reported as the ratio between the mean of the inter-regional pair tree-distance and the mean of the intra-regional pair tree distances across both regions.

Supplemental Figures

Figure S1. 25th, median (solid line), and 75th percentiles of the silhouette score distribution for 100 stochastically initiated rounds of k-means clustering for 2-16 clusters and a projection of the 3D embedding of the pairwise Hamming distance matrix between SARC-CoV-2 genomes. Partitions are color-coded and wires enclose the convex hulls for each of the five optimal clusters.

Figure S2. A. Distributions of the moving average, respecting segment boundaries, across a 100 codon window for synonymous (blue) and nonsynonymous (amino acid replacing) substitutions (orange). Solid lines: normal approximations of the distributions (same median and interquartile distance); solid lines: approximation with the same median and theoretical (Poisson) variance. **B.** Moving averages, respecting segment boundaries, across a 100 codon window for synonymous and nonsynonymous substitutions per site, raw (top) and normalized by the median (bottom). There are several regions in the genome with an apparent dramatic excess of synonymous substitutions: 5' end of orf1ab gene; most of the M gene; 3'-half of the N gene, as well as amino acid substitutions: most of the orf3a gene; most of the orf7a gene; most of the orf8 gene; and several regions in of the N gene.

Figure S3. Moving average over a window of 1000 codons, not respecting segment boundaries, of the total number of nucleotide exchanges n1->n2 summed over all substitutions. The ratio to the median over the entire alignment is also displayed as well as the normalized exchange distribution *(i.e.* #c->u/(#c->u+#c->g+#c->a)).

Figure S4 A. Two dimensional embedding of the Euclidean distances between the log-odds vectors of low and high frequency, nonsynonymous and synonymous mutations in the space of trinucleotide contexts relative to background expectation. The context of the high-frequency events (both S and N) is dramatically different from the background frequencies. There is a strong common component in the deviation of both kinds of high-frequency events. The context of the low-frequency events (both S and N) also differs slightly, in the same direction, from the background frequencies. There is a consistent distinction between synonymous and non-synonymous events, suggesting that a single mutagenic context or mechanistic bias does not account for both S and N events. **B.** Log odds ratio of low and high frequency mutations, both synonymous and nonsynonymous, relative to background expectation for each trinucleotide context. The NCN context (i.e. all mutations C->D) harbors dramatically more mutation events than the other contexts (all 16 NCN events are within the top 20 most-biased high-frequency events). The log-odds ratios for low-frequency events are poorly correlated with those for high-frequency events, suggesting that different mechanisms may be responsible for the strong bias observed among high frequency events and the weaker bias observed among low frequency events. **C.** Log odds ratio of high frequency nonsynonymous mutations

relative to the background expectation from the sum of both high synonymous and high nonsynonymous mutations vs. the sum + 1. There are 20 contexts where synonymous and non-synonymous events differ significantly (chi-sq> 11.28). 2/9 contexts with an excess of non-synonymous events are NCN (gct,tct). The remaining 7 are NGN (agt,gga,aga,ggt,agc,tgt). This additionally suggests that these non-synonymous events could be driven by other mechanisms. There is no correlation between the frequency of event context and the log-odds ratio for non-synonymous events, further suggesting that the log-odds ratio is not biased by hot-spot mutation context.

Figure S5. Correspondence between the “tree length for dN”, “tree length for dS”, and *dN/dS* between PAML and the results of the ancestral reconstruction utilizing Fitch traceback across 24 ORFs. Three high outliers in the PAML tS distribution are identified in the third plot and omitted from the first two.

Figure S6. A. The number of nonsynonymous events vs the number of synonymous events per codon. **B.** The moving average of 100 codons, respecting segment boundaries. **C.** The moving average after removing outlier high frequency events. Rho refers to Spearman. Dashed lines are 2/1.3*x reflecting the genome-wide ratio of nonsynonymous to synonymous substitutions, solid lines are linear best fit. Red points correspond to the middle third of the N protein.

Figure S7. Moving averages across a 100 codon window for synonymous and nonsynonymous substitutions per site in the N protein after removing outlier high frequency events. The nonsynonymous substitution frequencies in the center of the protein are not elevated relative to either terminus.

Figure S8. The fraction of sites with at least one substitution vs moving averages, respecting segment boundaries, over windows of 100 codons for synonymous and nonsynonymous substitutions.

Figure S9. Site history trees for spike 69 as drawn in Fig. 1C.

Figure S10. Epistatic network for the tree including mutations with NCN context and meeting all other criteria for positive selection. Mutations in the polyprotein are not displayed.

Figures S11. Correlation between sequencing date and tree distance to the root for all isolates with metadata as well as those which appear explicitly in the tree.

Figures S12-14. Global distribution of sequences. Color represents the number of sequences from that location and size represents the fraction of sequences from the clade displayed. Partition indices are in the top left corner of each map.

Figure S15. Regional SARS-CoV-2 partition dynamics during the COVID-19 pandemic (absolute number of sequences shown in contrast to Fig. 2).

Figure S16. The mean tree distance between pairs of isolates **A.** from different regions, **B.** within the same region (averaged over both regions in each pair) and **C.** The ratio over time (see Methods). 25th, 50th, and 75th percentiles of all 15 pairs of 6 regions. The ratio reported is between the mean of the inter-regional pair tree-distance and the mean of the intra-regional pair tree distances across both regions for each pair of regions.

Figure S17. Regional distributions of major partitions in the global topology March vs. July and July vs. November.

Figure S18. The frequencies of NLS-associated mutations N|194L, N119L, N203K, N205I, and N220V over time and across geographic regions along with S|614G for reference.

Figure S19. The Kullback-Leibler divergence and sequence logo for the 15 most divergent codons in sequences sourced after October 15, 2020 from Oceania in partition 7 vs. all sequences from Oceania in partition 7.

Figure S20. The Kullback-Leibler divergence and sequence logo for the 15 most divergent codons in sequences sourced after November 1, 2020 from Oceania in partition 6 vs. all sequences from Oceania in partition 6.

Figure S21. The Kullback-Leibler divergence and sequence logo for the 15 most divergent codons in sequences sourced after November 1, 2020 from Africa in partition 6 vs. all sequences from Africa in partition 6.

Figures S22-24. The frequencies of variant-associated mutations in the spike protein over time and geographic regions.

Figure S25. Regional SARS-CoV-2 variant clade dynamics during the COVID-19 pandemic (log of absolute number of sequences shown).

Supplemental Tables

Table S1. The list of all mutations either in the top 100 most commonly observed or top 100 with the greatest number of parallel substitutions ordered as they appear in the genome.

Table S2. List of sites most likely to be evolving under positive selection. For List 2 the average tree fraction descendant from each candidate positively selected amino acid replacement must be sufficiently large(see Methods).

Table S3. All epistatic interactions among states meeting the criteria outlined in the main text for likely positive selection with binomial/Poisson scores greater than 5 or at least 2 simultaneous substitutions. Each mutation must have a minimum weight of approximately 200 leaves and each pair, 100 leaves. Each pair is arbitrarily ordered and the numbers of simultaneous, descendant, and independent substitutions are tabulated.

Table S4. List 1. List of variant mutations and variant IDs sorted by the number of variant ID's assigned to each mutation. **List 2**. List of all pairs of mutations associated with a single variant ID (internal variant ID's excluded. **List 3**. List of putative epistatic interactions between variant mutations and other states in the tree.

Table S5. The number of isolates (out of approximately 175k) observed to bear at least one substitution relative to the reference sequence, NC_045512.2, within the regions specified. These regions are commonly used within PCR assays for diagnostic testing.

References

1. Elbe S & Buckland-Merrett G (2017) Data, disease and diplomacy: GISAID's innovative contribution to global health. *Global Challenges* 1(1):33-46.
2. Benson DA, *et al.* (2012) GenBank. *Nucleic acids research* 41(D1):D36-D42.
3. Zhao W-M, *et al.* (2020) The 2019 novel coronavirus resource. *Yi chuan= Hereditas* 42(2):212-221.
4. Fu L, Niu B, Zhu Z, Wu S, & Li W (2012) CD-HIT: accelerated for clustering the next-generation sequencing data. *Bioinformatics* 28(23):3150-3152.
5. Li W & Godzik A (2006) Cd-hit: a fast program for clustering and comparing large sets of protein or nucleotide sequences. *Bioinformatics* 22(13):1658-1659.
6. Katoh K, Misawa K, Kuma Ki, & Miyata T (2002) MAFFT: a novel method for rapid multiple sequence alignment based on fast Fourier transform. *Nucleic acids research* 30(14):3059-3066.
7. Price MN, Dehal PS, & Arkin AP (2010) FastTree 2–approximately maximum-likelihood trees for large alignments. *PloS one* 5(3):e9490.
8. Nguyen L-T, Schmidt HA, Von Haeseler A, & Minh BQ (2015) IQ-TREE: a fast and effective stochastic algorithm for estimating maximum-likelihood phylogenies. *Molecular biology and evolution* 32(1):268-274.
9. Morel B, *et al.* (2020) Phylogenetic analysis of SARS-CoV-2 data is difficult. *bioRxiv*.
10. Fitch WM (1971) Toward defining the course of evolution: minimum change for a specific tree topology. *Systematic Biology* 20(4):406-416.
11. Rochman ND, Wolf YI, & Koonin EV (2020) Deep phylogeny of cancer drivers and compensatory mutations. *Communications biology* 3(1):1-11.
12. MathWorks I (1992) *MATLAB, high-performance numeric computation and visualization software: reference guide* (MathWorks).
13. Yang Z (2007) PAML 4: phylogenetic analysis by maximum likelihood. *Molecular biology and evolution* 24(8):1586-1591.
14. Simplemaps (World Cities Database.

S1

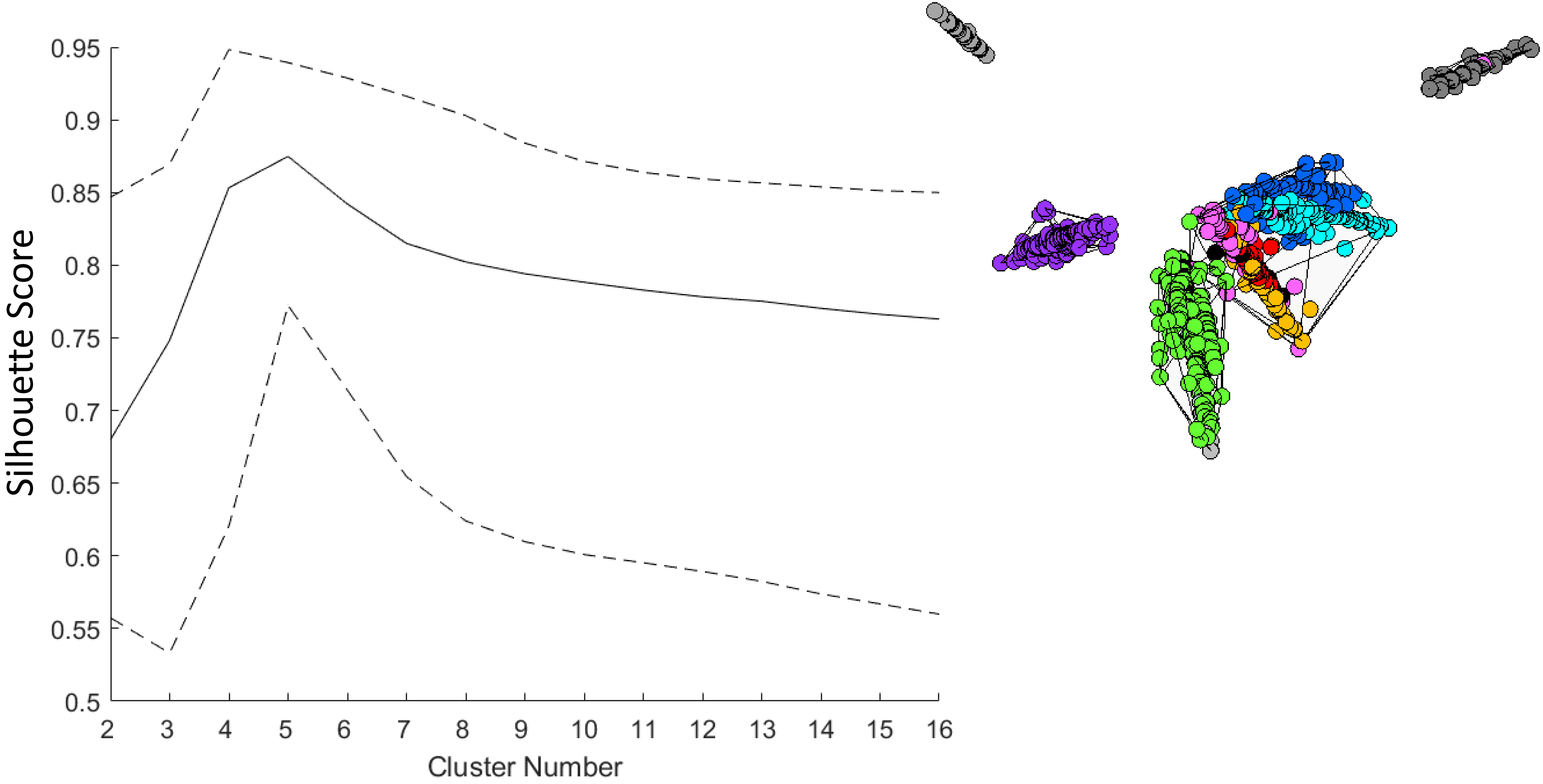
Silhouette Score
0.95
0.9
0.85
0.8
0.75
0.7
0.65
0.6
0.55
0.5
2
3
4
5
6
7
8
9
10
11
12
13
14
15
16
Cluster Number

S2

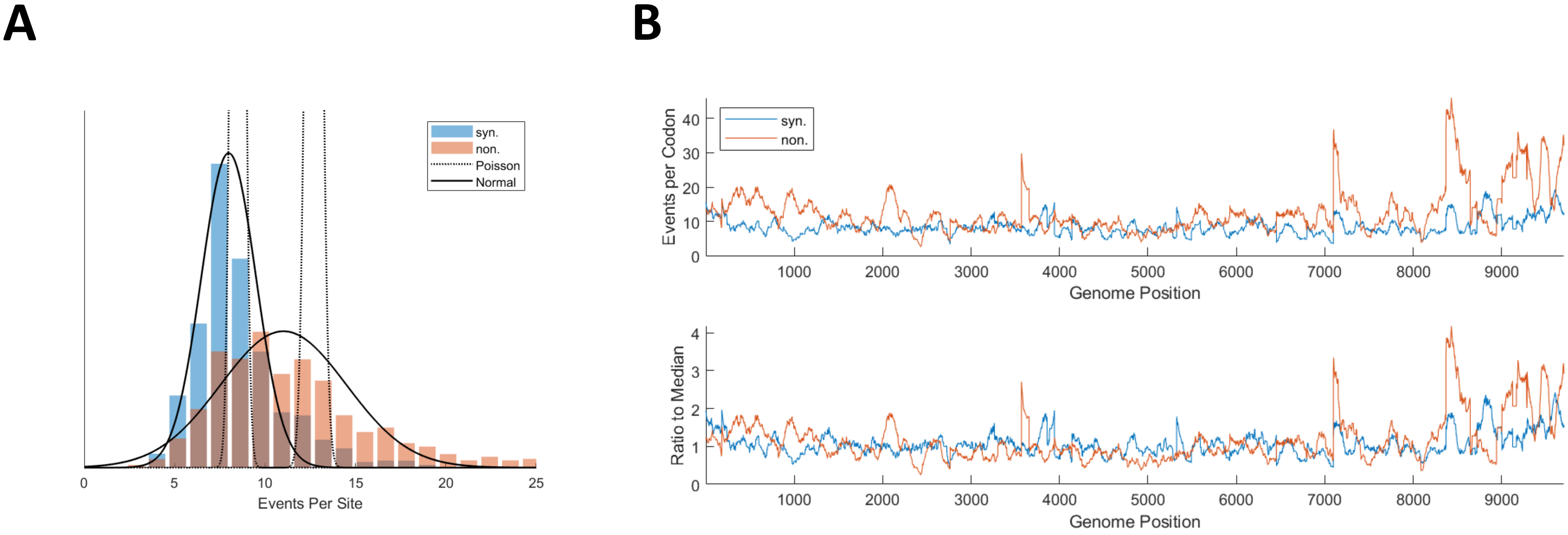

A
syn.
non.
Poisson
Normal
0
5
10
15
20
25
Events Per Site
B
Events per Codon
40
30
20
10
0
syn.
non.
1000
2000
3000
4000
5000
6000
7000
8000
9000
Genome Position
Ratio to Median
4
3
2
1
0
1000
2000
3000
4000
5000
6000
7000
8000
9000
Genome Position

S3

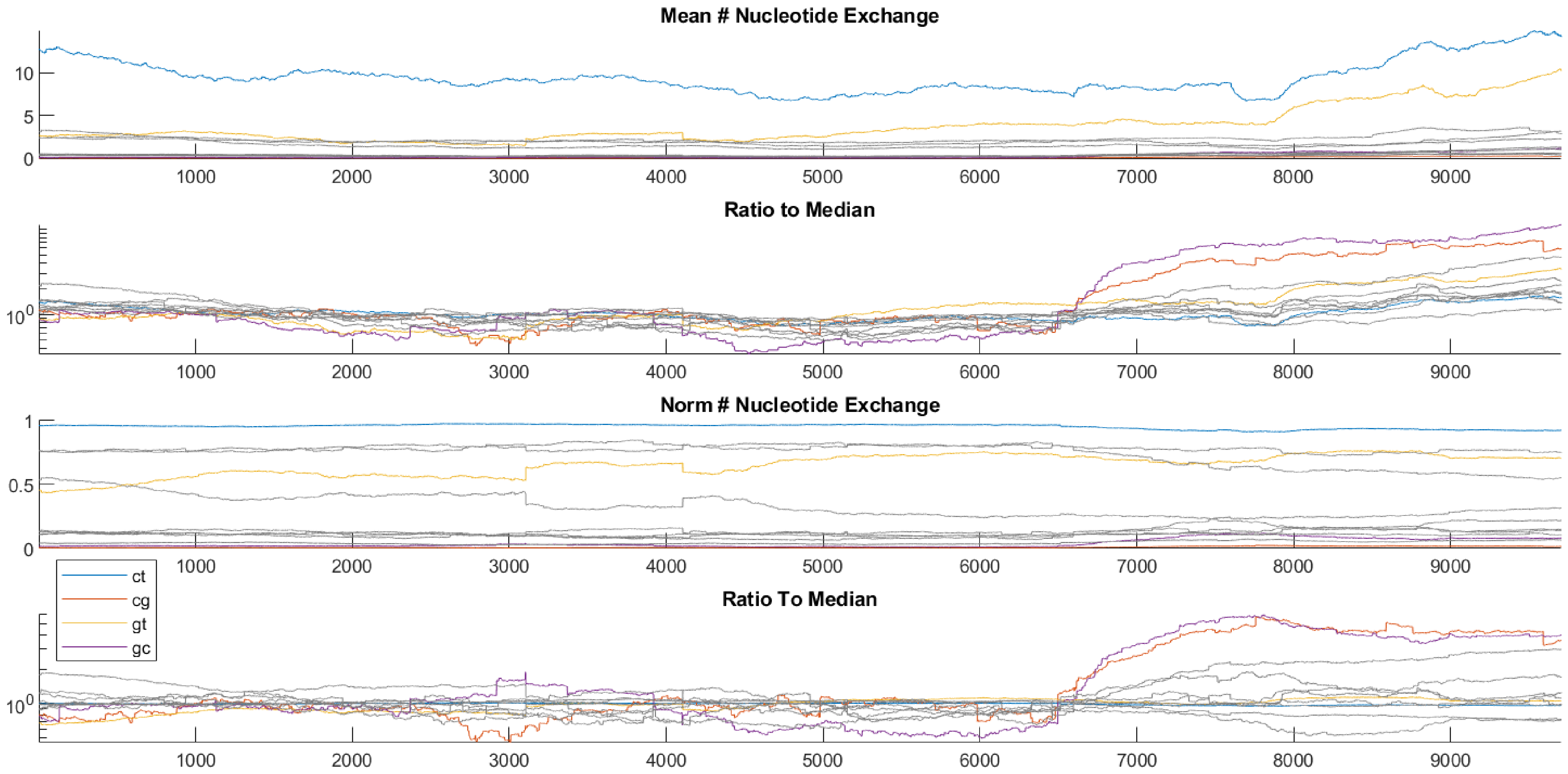
Mean # Nucleotide Exchange
10
5
0
1000
2000
3000
4000
5000
6000
7000
8000
9000
Ratio to Median
10^0
1000
2000
3000
4000
5000
6000
7000
8000
9000
Norm # Nucleotide Exchange
1
0.5
0
1000
2000
3000
4000
5000
6000
7000
8000
9000
ct
cg
gt
gc
Ratio To Median
10^0
1000
2000
3000
4000
5000
6000
7000
8000
9000

S4

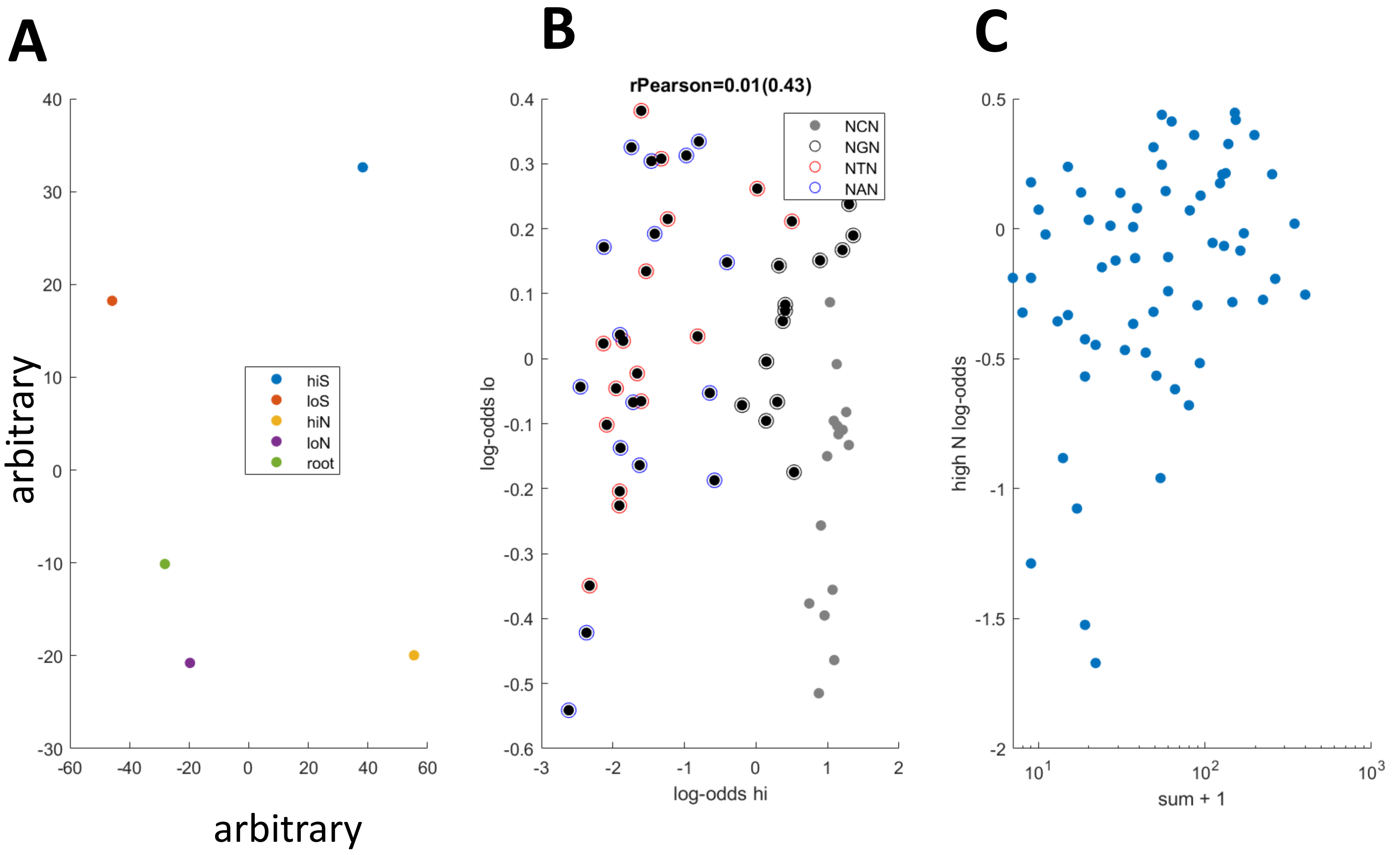

context	log-odd S	log-odd N	chi-sq
agt	-2.04	0.45	72.63
gga	-2.13	0.44	26.41
aga	-1.63	0.42	62.85
ggt	-1.68	0.41	25.9
tgt	-1.09	0.36	55.91
agc	-1.14	0.36	25.07
tgc	-0.9	0.33	30.98
gct	-0.42	0.21	19.83
tct	0.26	-0.19	14.04
aca	0.32	-0.25	34.32
tca	0.34	-0.27	21.31
cca	0.34	-0.28	14.46
atc	0.5	-0.52	23.85
gcg	0.51	-0.57	14.36
tcg	0.54	-0.62	21.6
ata	0.58	-0.68	30.33
atg	0.67	-0.96	31.4
cta	0.76	-1.52	16.31
ttg	0.79	-1.67	20.8

S5

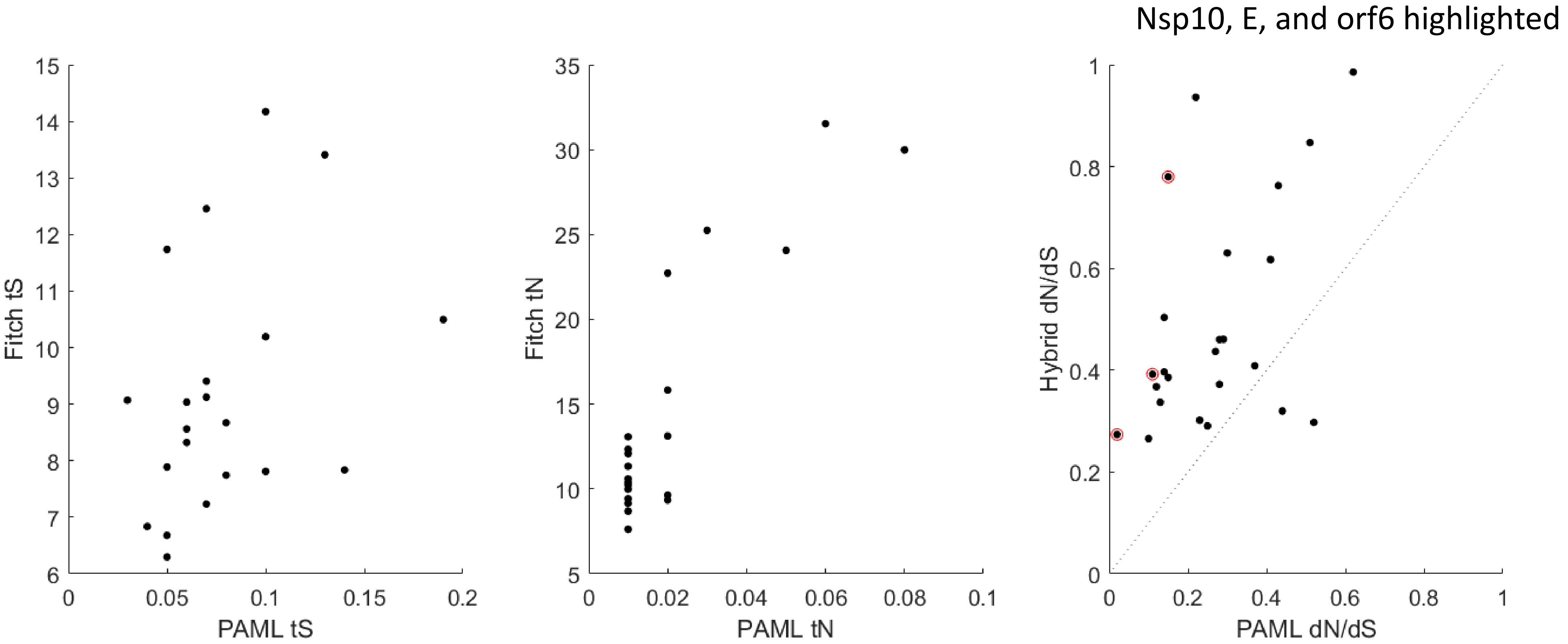
Nsp10, E, and orf6 highlighted
Fitch tS
PAML tS
15
14
13
12
11
10
9
8
7
6
0
0.05
0.1
0.15
0.2
Fitch tN
PAML tN
35
30
25
20
15
10
5
0
0.02
0.04
0.06
0.08
0.1
Hybrid dN/dS
PAML dN/dS
1
0.8
0.6
0.4
0.2
0
0
0.2
0.4
0.6
0.8
1

S6

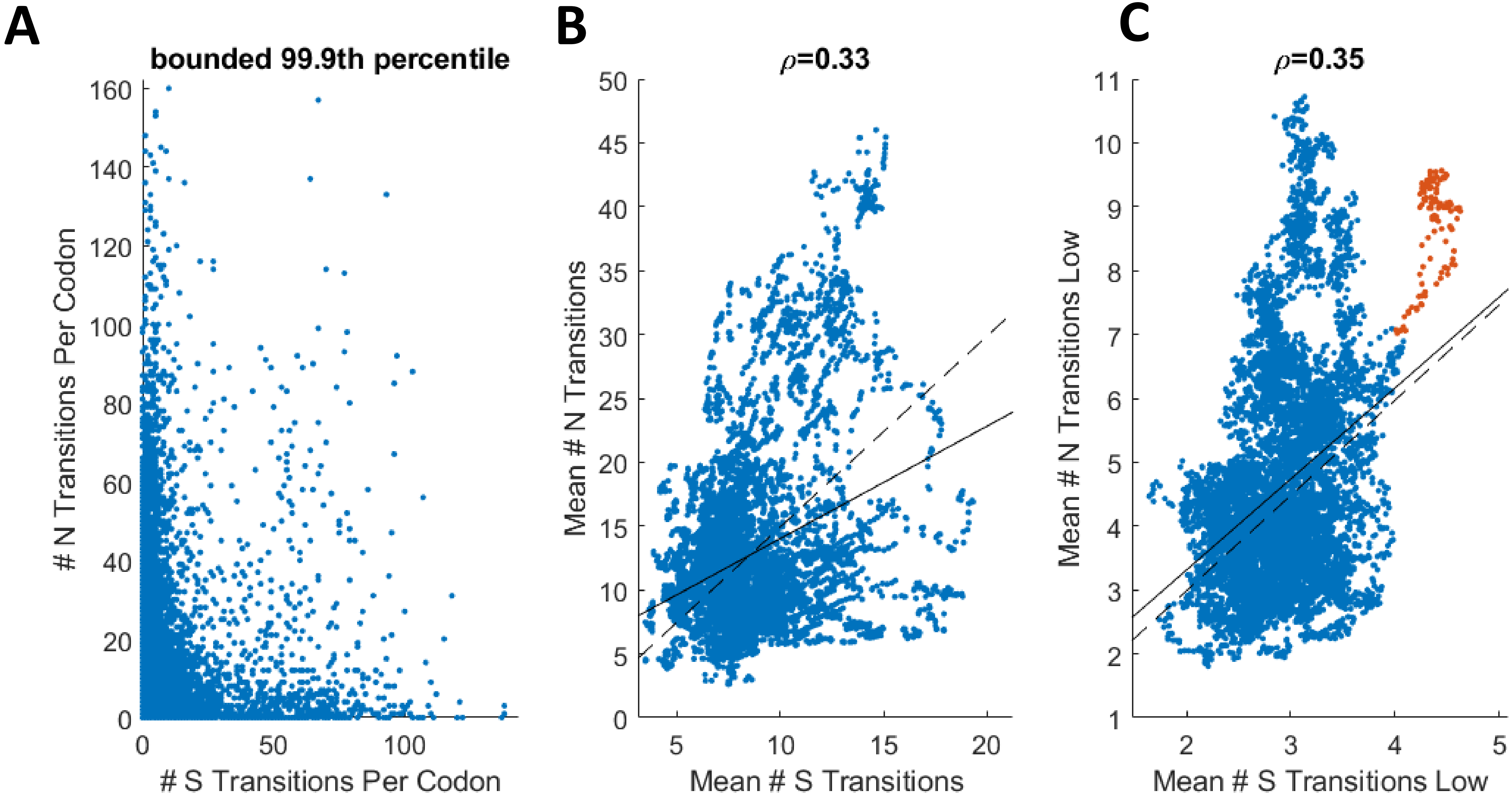

A
bounded 99.9th percentile
# N Transitions Per Codon
# S Transitions Per Codon
0
20
40
60
80
100
120
140
160
0
50
100
B
ρ=0.33
Mean # N Transitions
Mean # S Transitions
0
5
10
15
20
25
30
35
40
45
50
5
10
15
20
C
ρ=0.35
Mean # N Transitions Low
Mean # S Transitions Low
1
2
3
4
5
6
7
8
9
10
11
2
3
4
5

S7

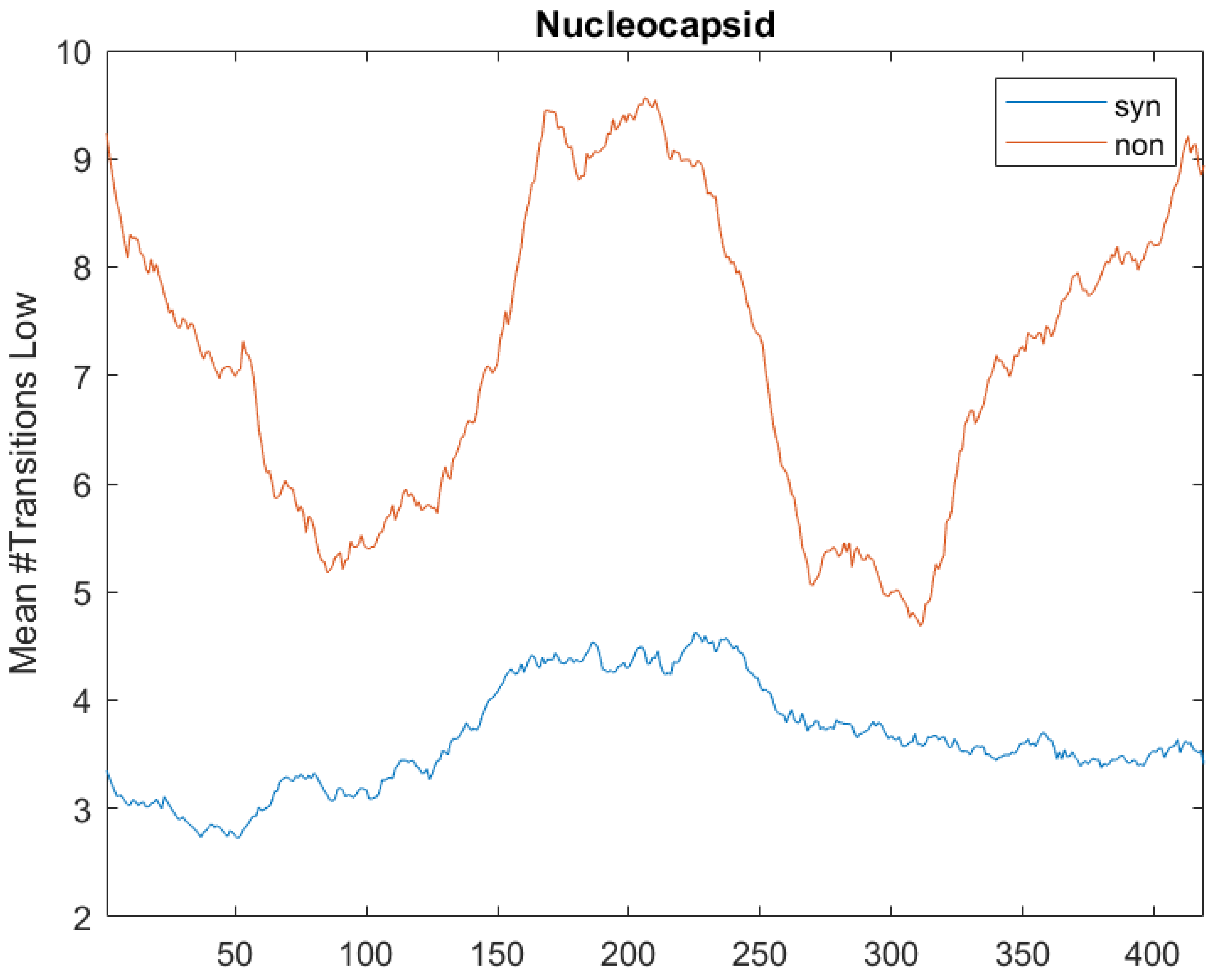
Nucleocapsid
Mean #Transitions Low
10
9
8
7
6
5
4
3
2
50
100
150
200
250
300
350
400
syn
non

S8

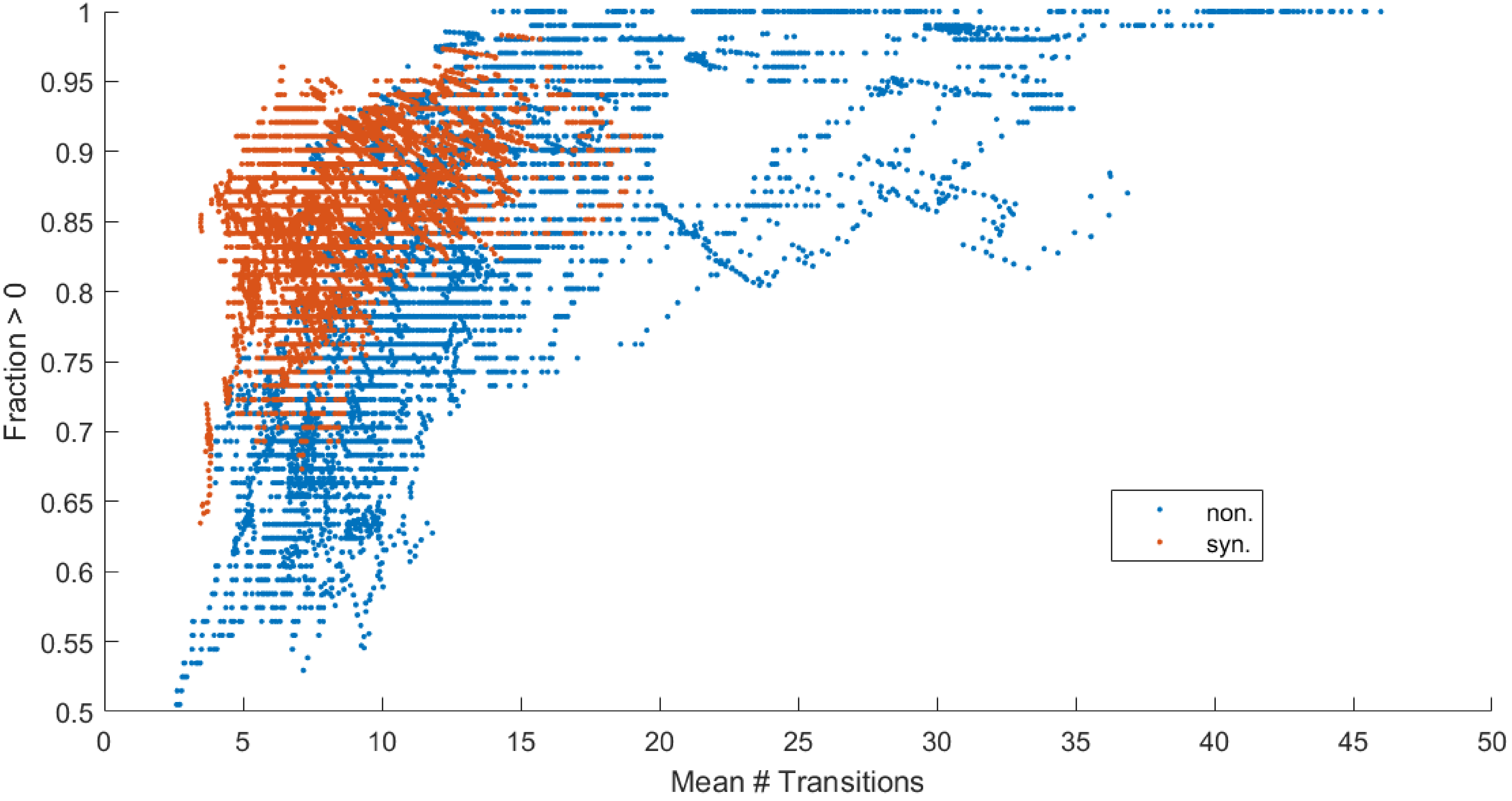
1
0.95
0.9
0.85
0.8
0.75
0.7
0.65
0.6
0.55
0.5
Fraction > 0
0
5
10
15
20
25
30
35
40
45
50
Mean # Transitions
non.
syn.

S9

S|69 -

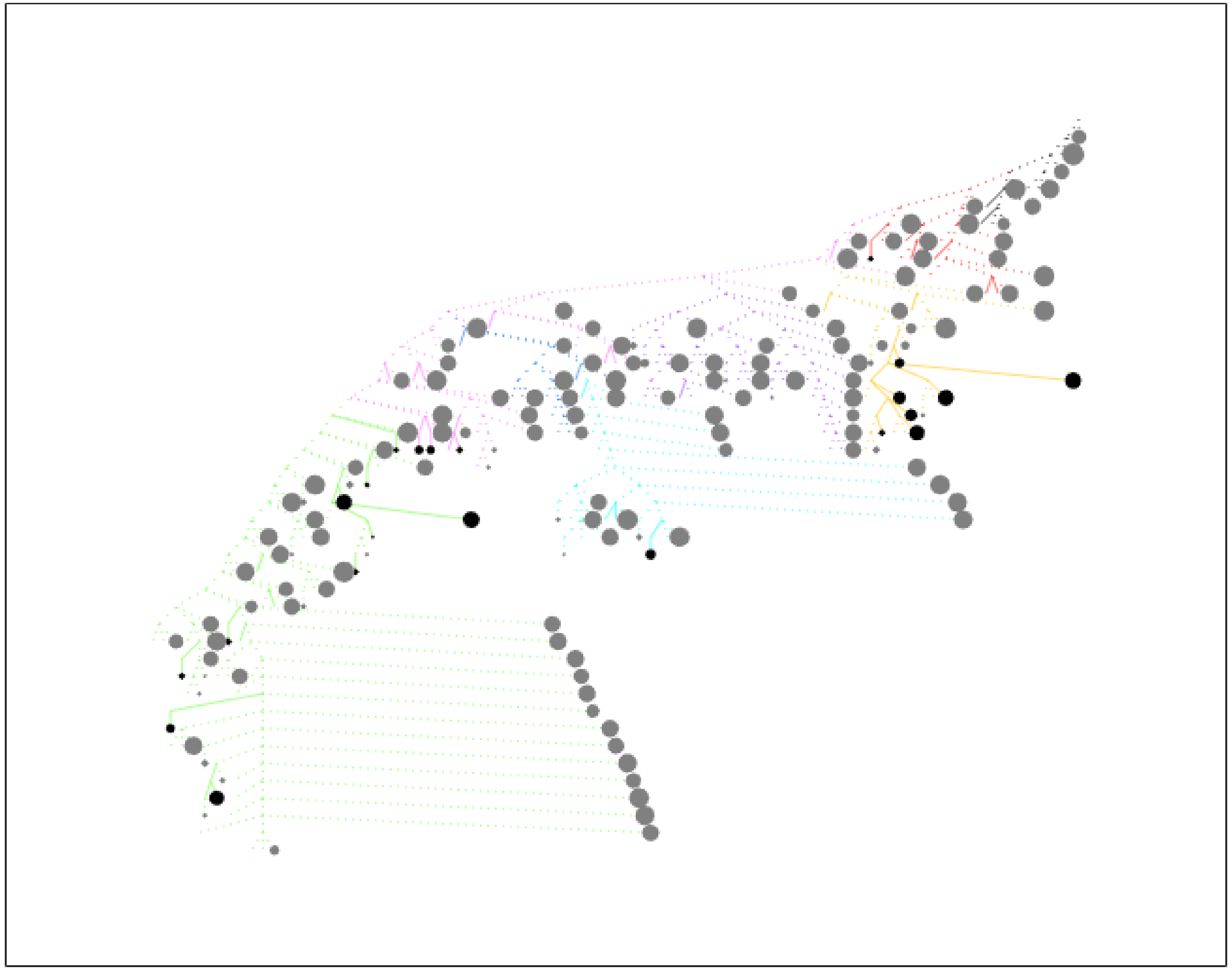

S10

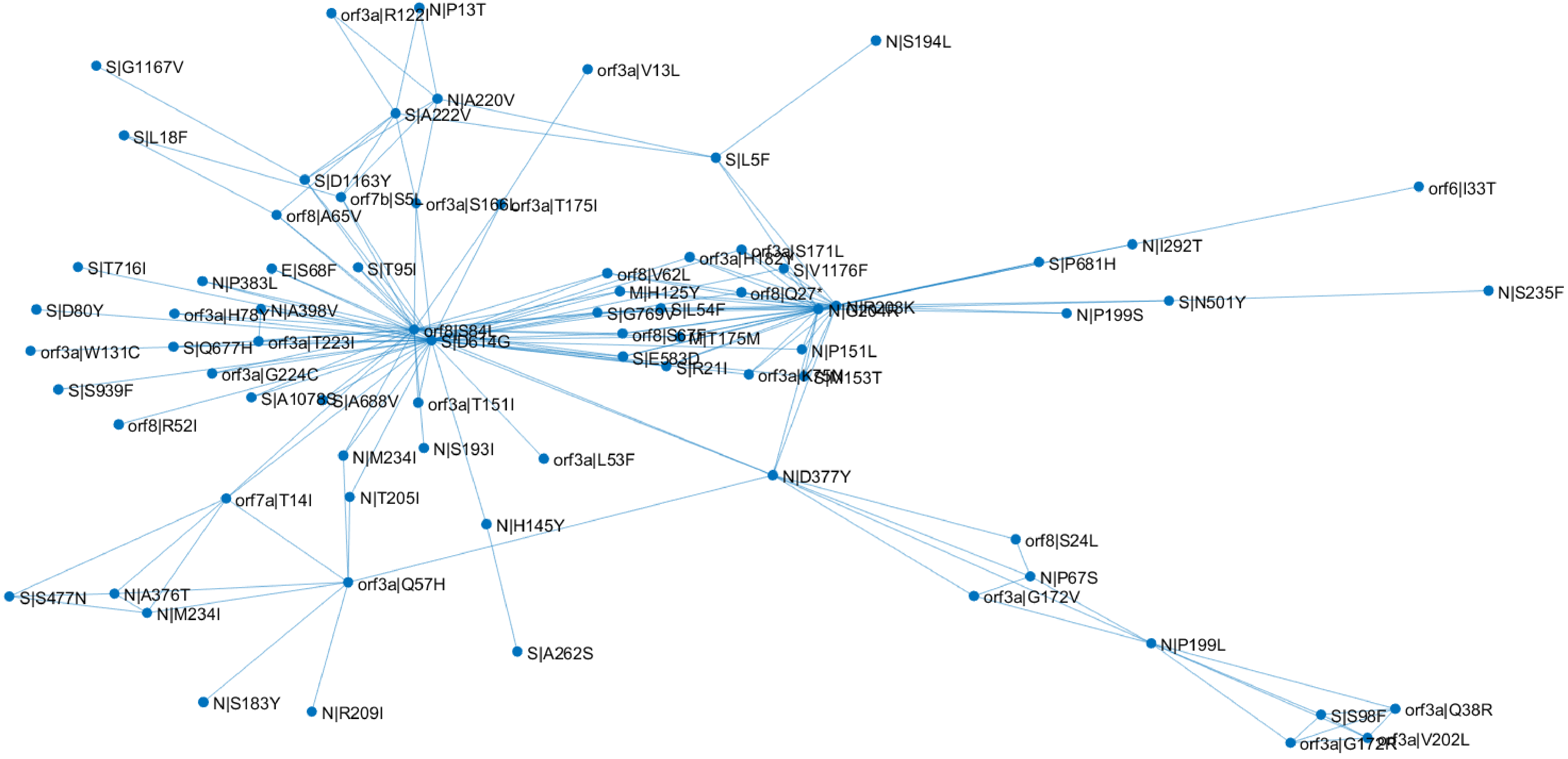

orf3a|R122I
N|P13T
S|G1167V
orf3a|V13L
N|S194L
N|A220V
S|A222V
S|L18F
S|L5F
S|D1163Y
orf7b|S5L
orf3a|S166L
orf3a|T175I
orf8|A65V
orf6|I33T
orf3a|S171L
orf3a|H182Y
N|I292T
S|V1176F
S|P681H
S|T716I
E|S68F
S|T95I
orf8|V62L
N|P383L
M|H125Y
orf8|Q27*
N|S235F
S|D80Y
N|A398V
S|G769V
S|L54F
N|R203K
N|G204R
S|N501Y
orf3a|H78Y
N|P199S
orf8|S84L
orf8|S67F
M|T175M
orf3a|T223I
S|D614G
orf3a|W131C
S|Q677H
N|P151L
S|E583D
S|R21I
orf3a|G224C
orf3a|K75N
S|M153T
S|S939F
S|A1078S
S|A688V
orf3a|T151I
orf8|R52I
N|S193I
N|M234I
orf3a|L53F
N|D377Y
orf7a|T14I
N|T205I
N|H145Y
orf8|S24L
N|P67S
orf3a|G172V
orf3a|Q57H
S|S477N
N|A376T
N|M234I
N|P199L
S|A262S
S|S98F
orf3a|Q38R
orf3a|G172R
orf3a|V202L
N|S183Y
N|R209I

S11

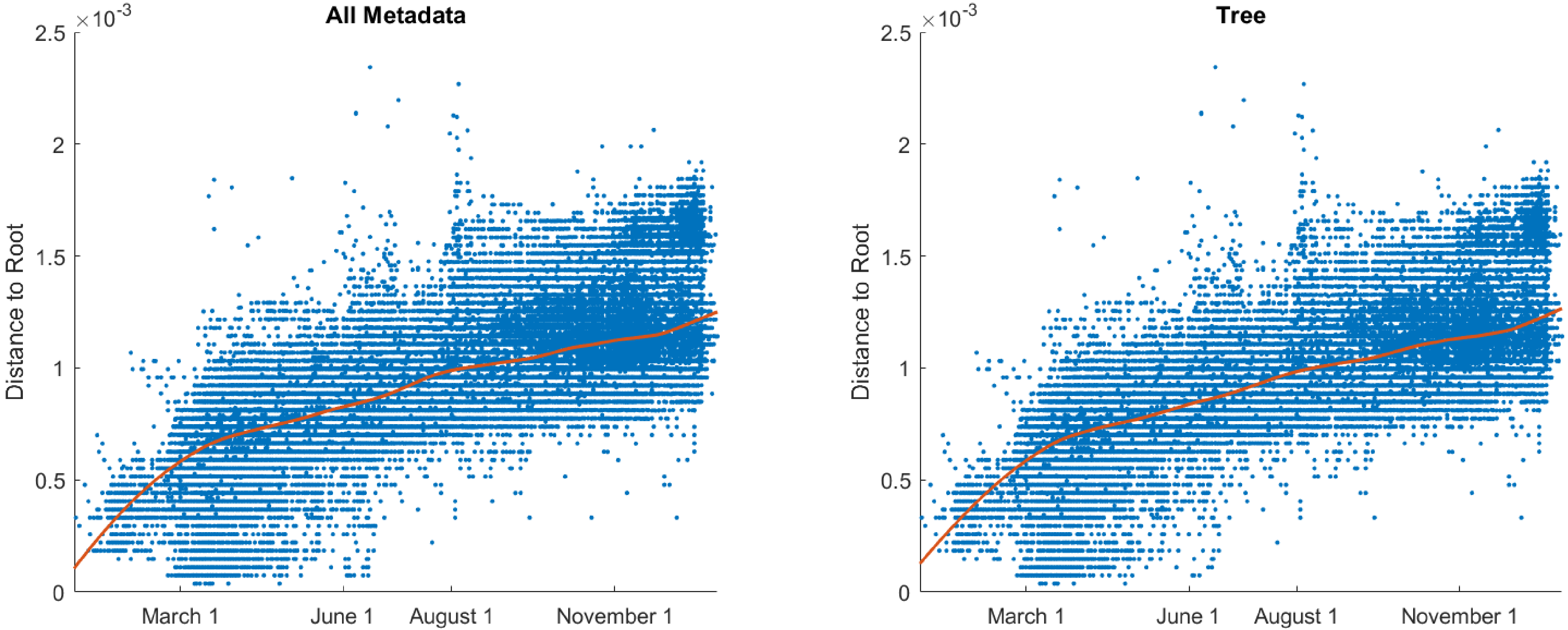
All Metadata
Tree
×10⁻³
Distance to Root
2.5
2
1.5
1
0.5
0
March 1
June 1
August 1
November 1

S12

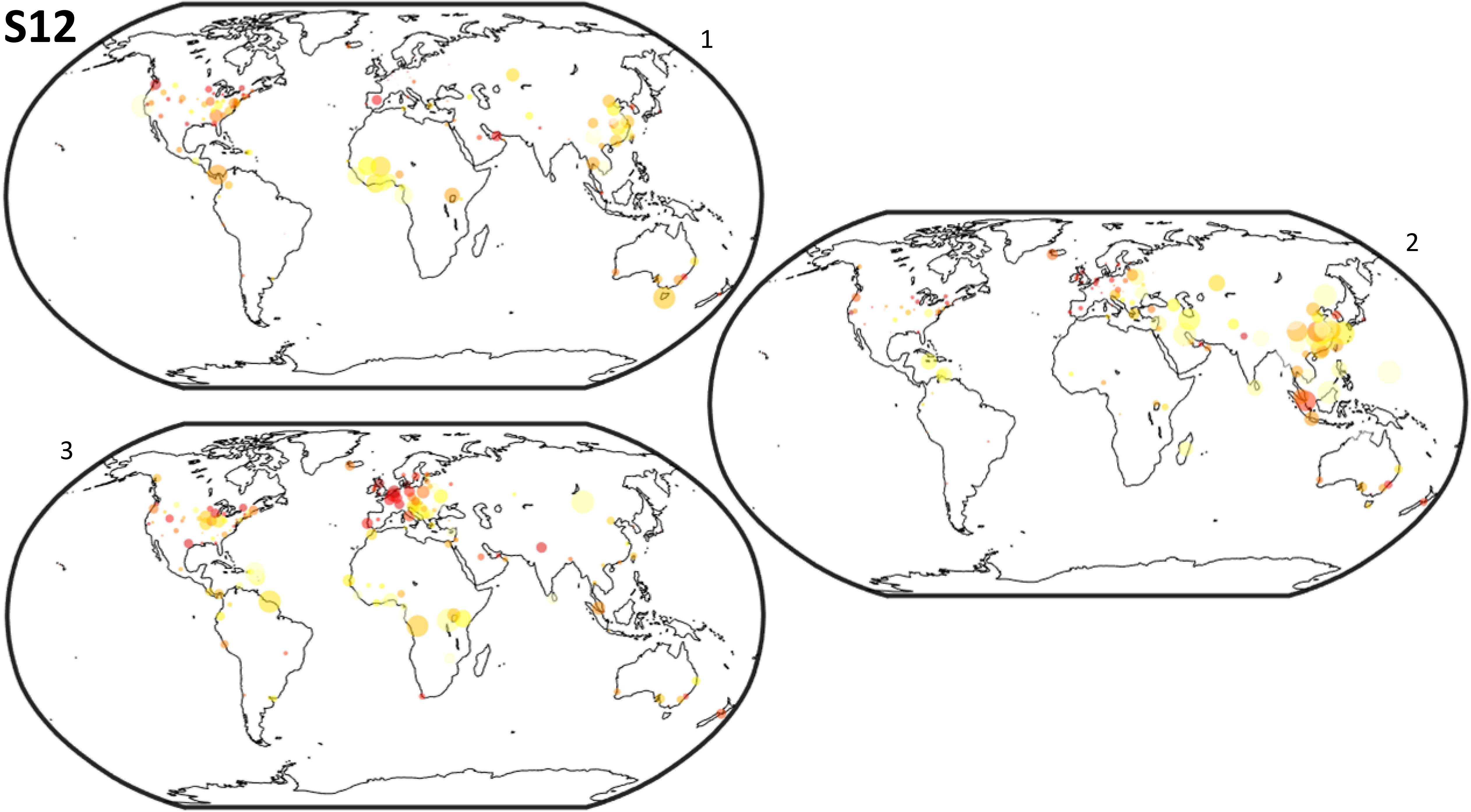

S13

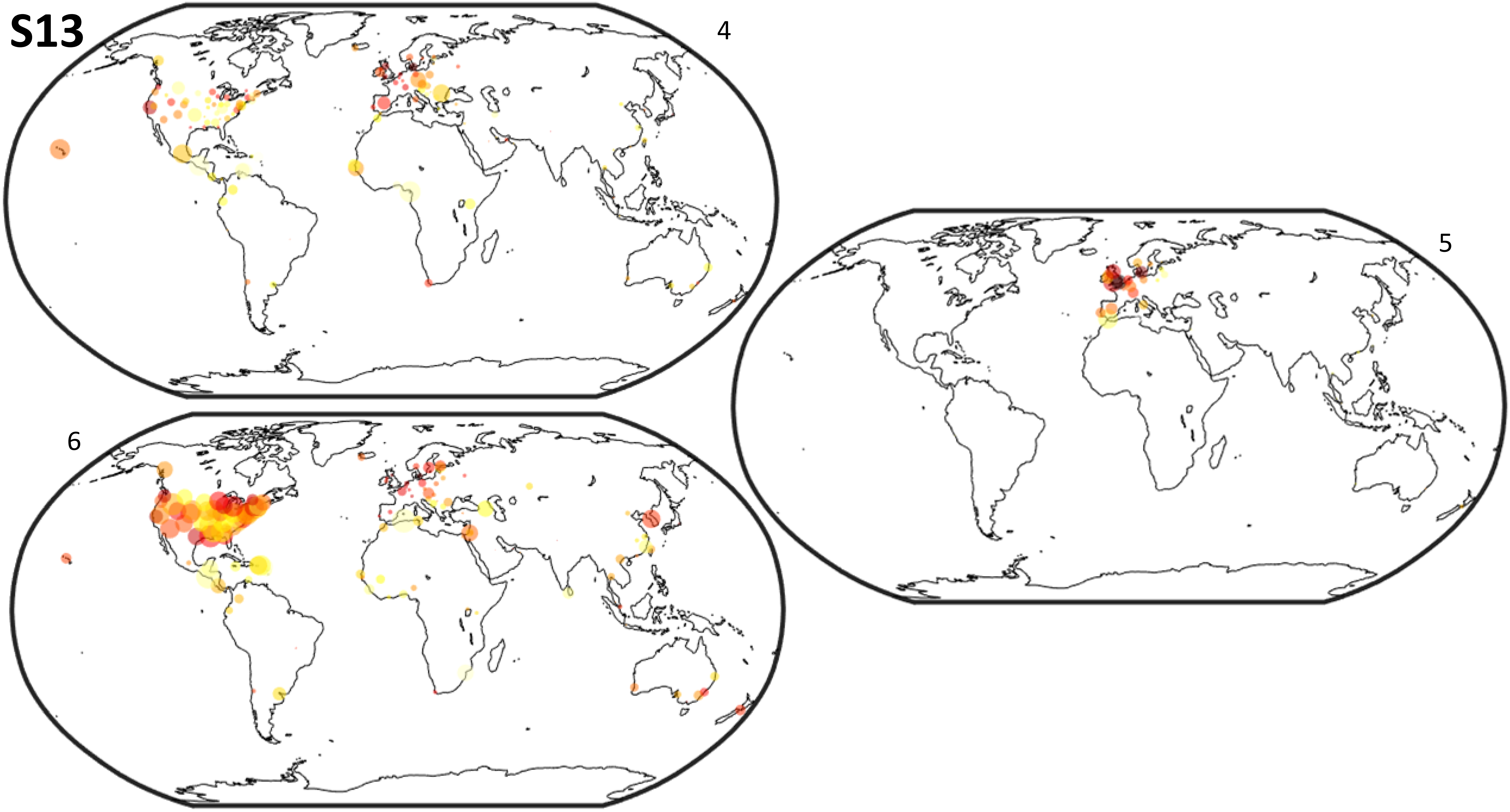

S14

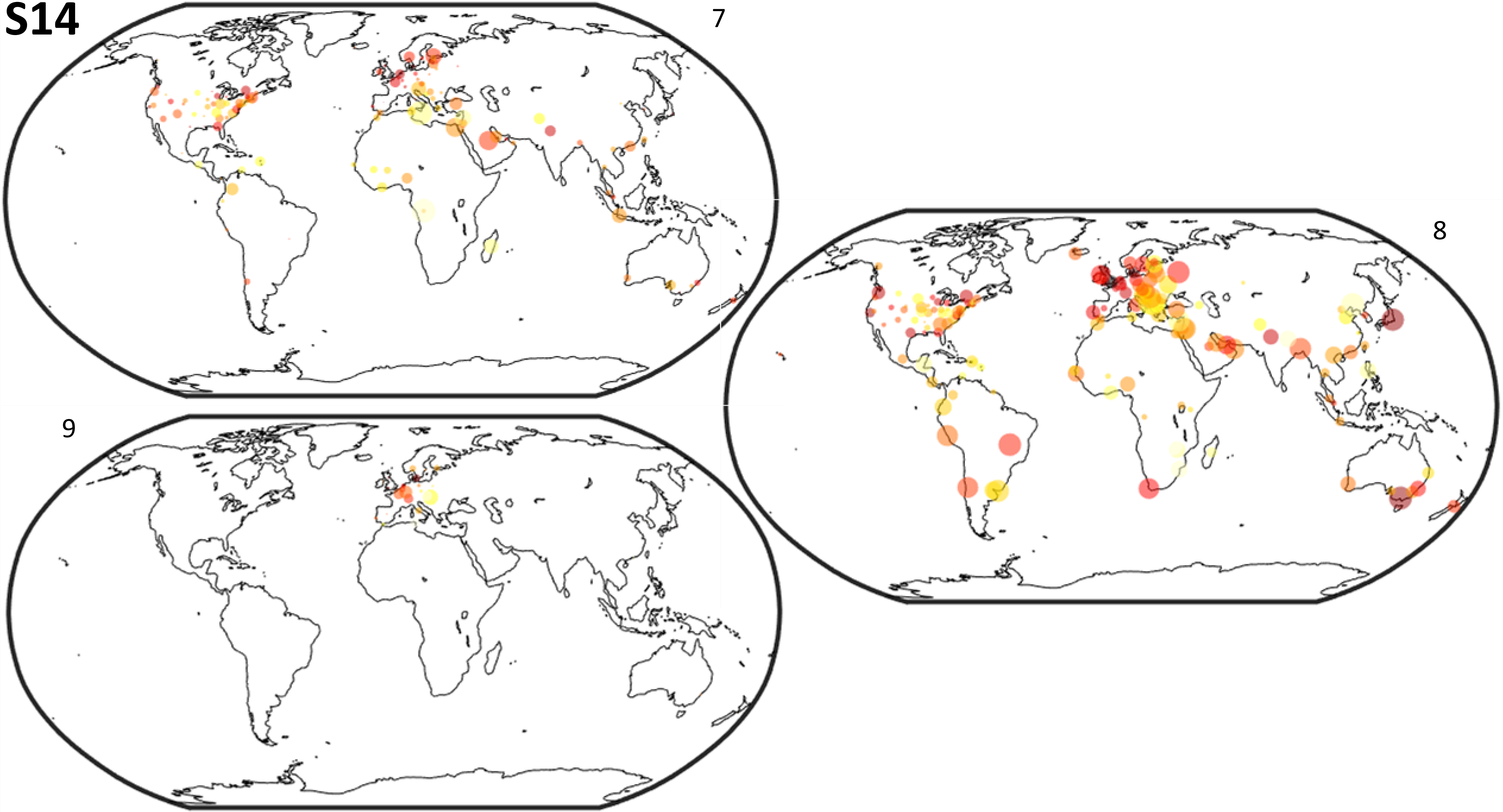

S15

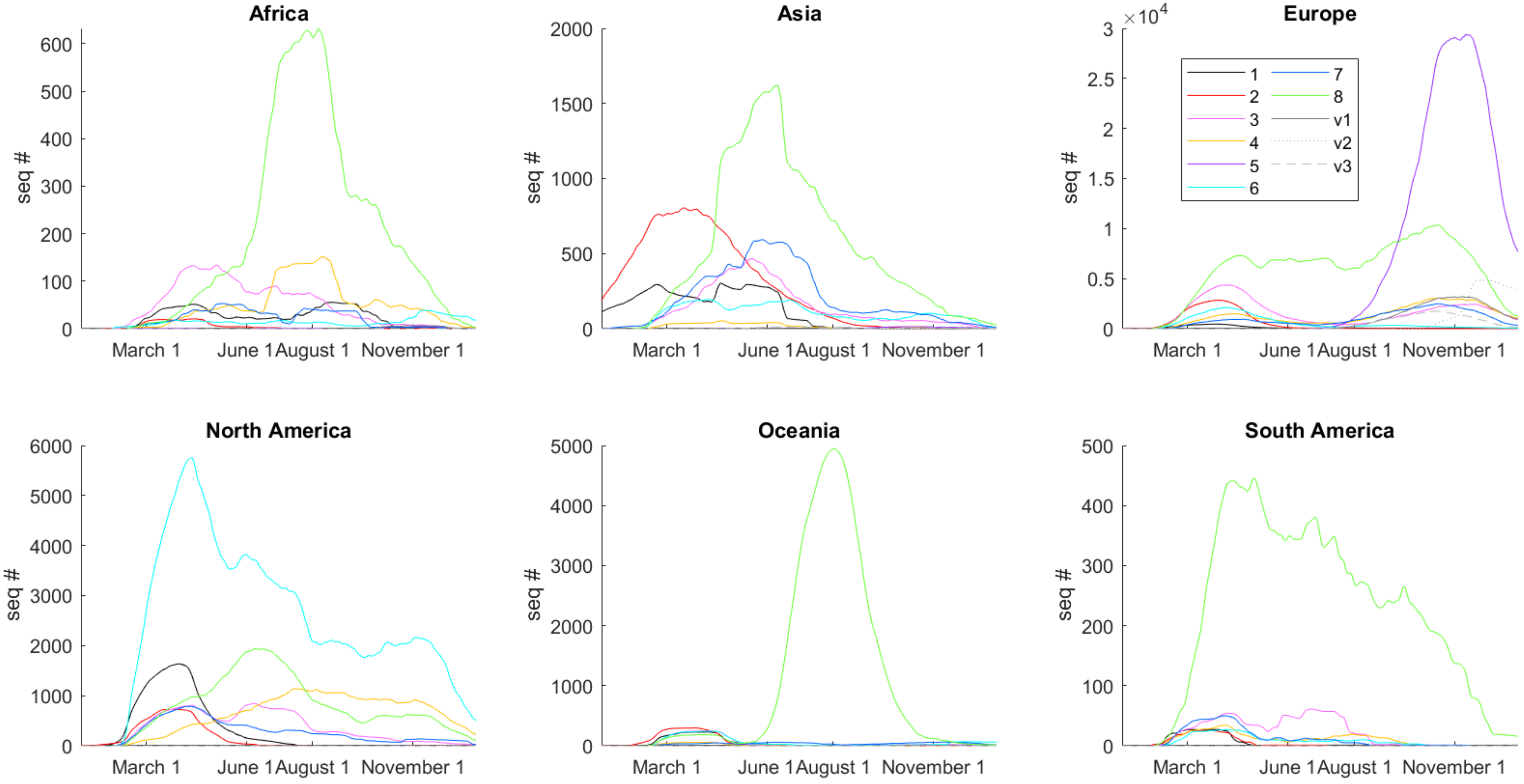
Africa
Asia
Europe
North America
Oceania
South America
seq #
$\times 10^4$
March 1
June 1
August 1
November 1
0
100
200
300
400
500
600
1000
1500
2000
3000
4000
5000
6000
0.5
1
1.5
2
2.5
3
1
2
3
4
5
6
7
8
v1
v2
v3

S16

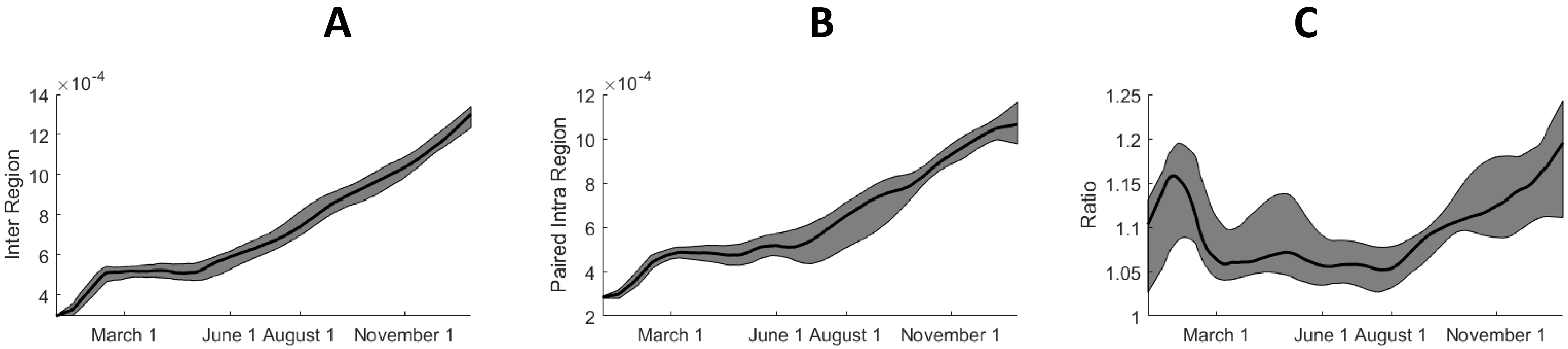
A
B
C
$\times 10^{-4}$
Inter Region
14
12
10
8
6
4
March 1
June 1
August 1
November 1
$\times 10^{-4}$
Paired Intra Region
12
10
8
6
4
2
March 1
June 1
August 1
November 1
Ratio
1.25
1.2
1.15
1.1
1.05
1
March 1
June 1
August 1
November 1

S17

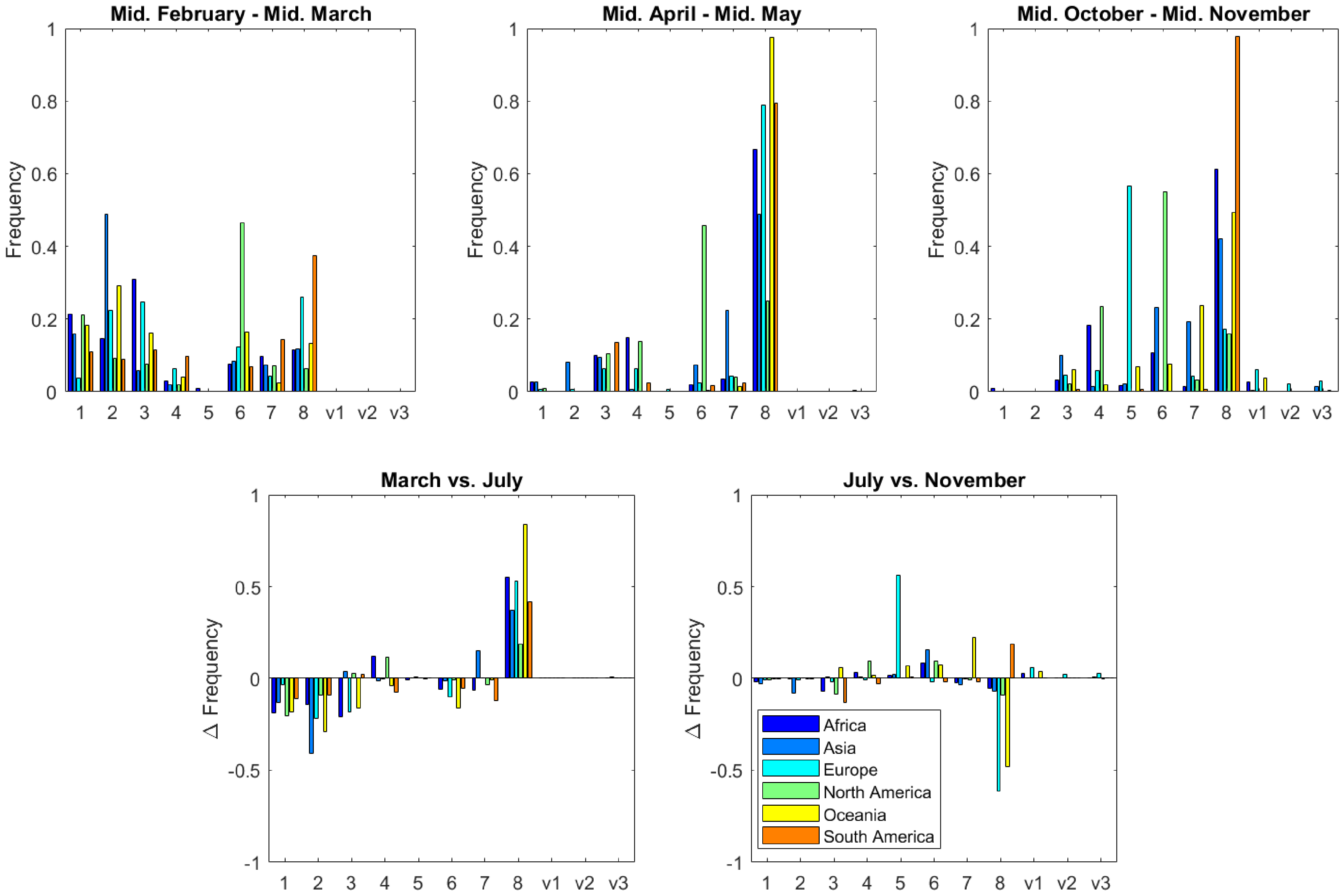
Mid. February - Mid. March
Mid. April - Mid. May
Mid. October - Mid. November
Frequency
0
0.2
0.4
0.6
0.8
1
1
2
3
4
5
6
7
8
v1
v2
v3
March vs. July
July vs. November
Δ Frequency
-1
-0.5
0
0.5
1
Africa
Asia
Europe
North America
Oceania
South America

S18

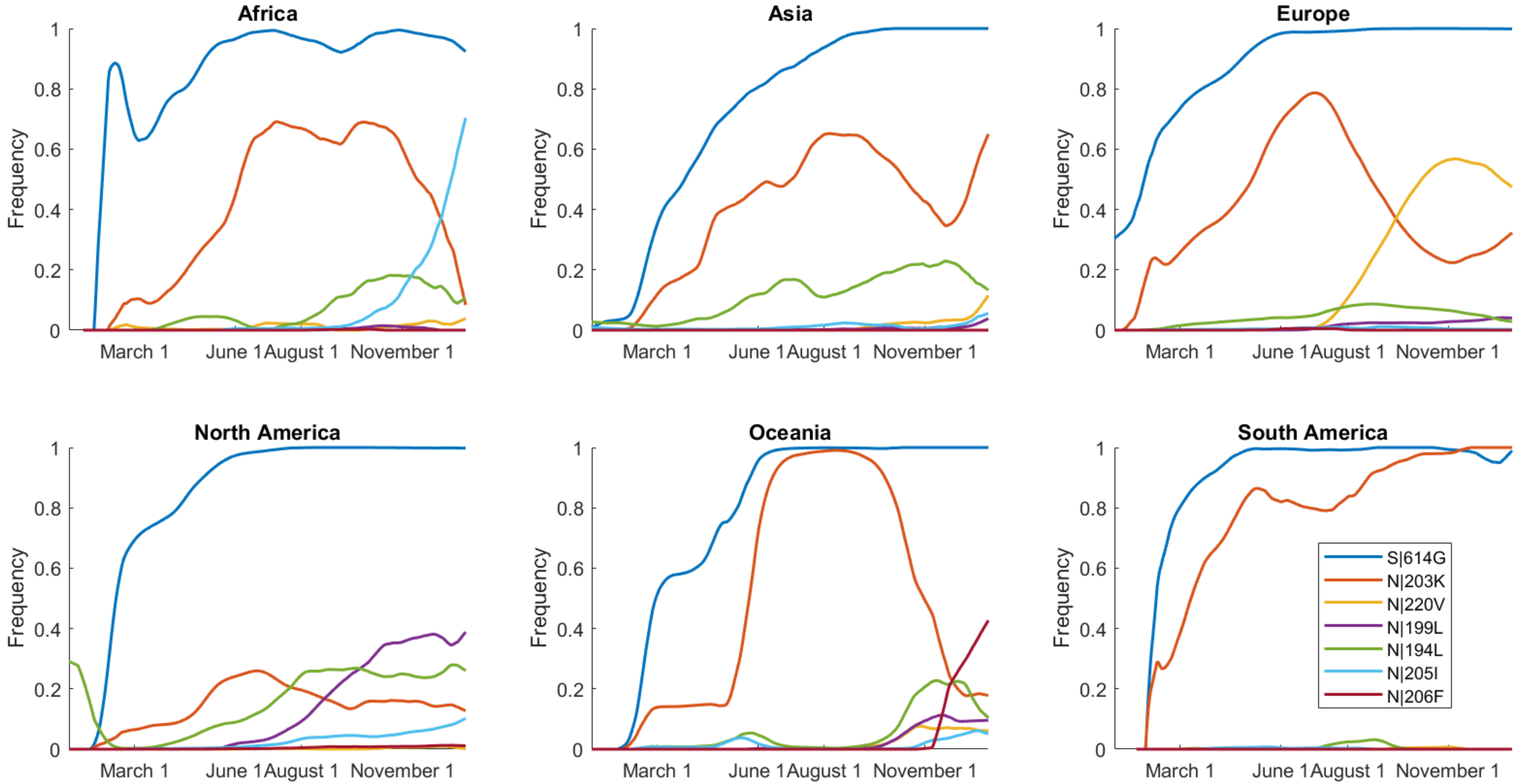

Africa
Asia
Europe
North America
Oceania
South America
Frequency
0
0.2
0.4
0.6
0.8
1
March 1
June 1
August 1
November 1
S|614G
N|203K
N|220V
N|199L
N|194L
N|205I
N|206F

S19

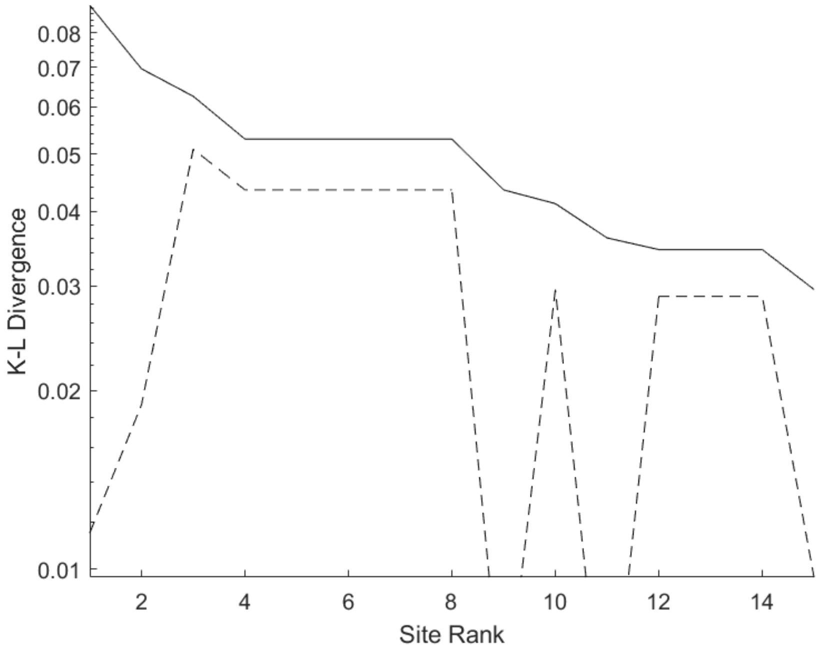

Partition 7, Late 2020, Oceania

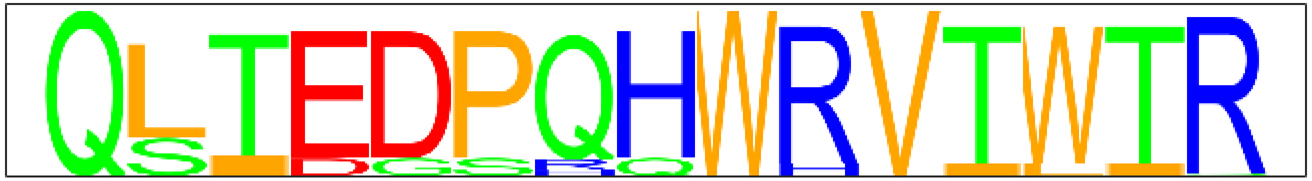

Partition 7, Oceania

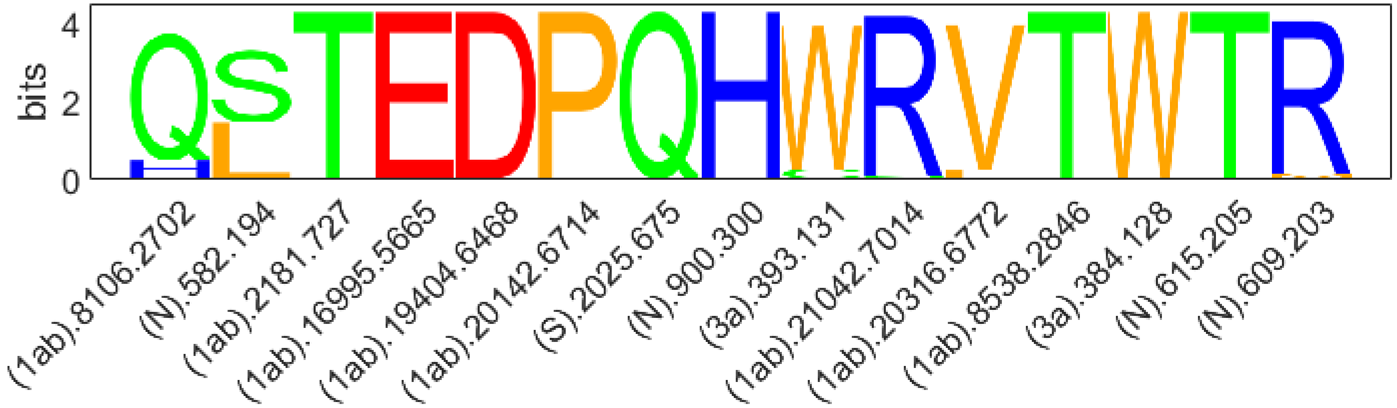

S20

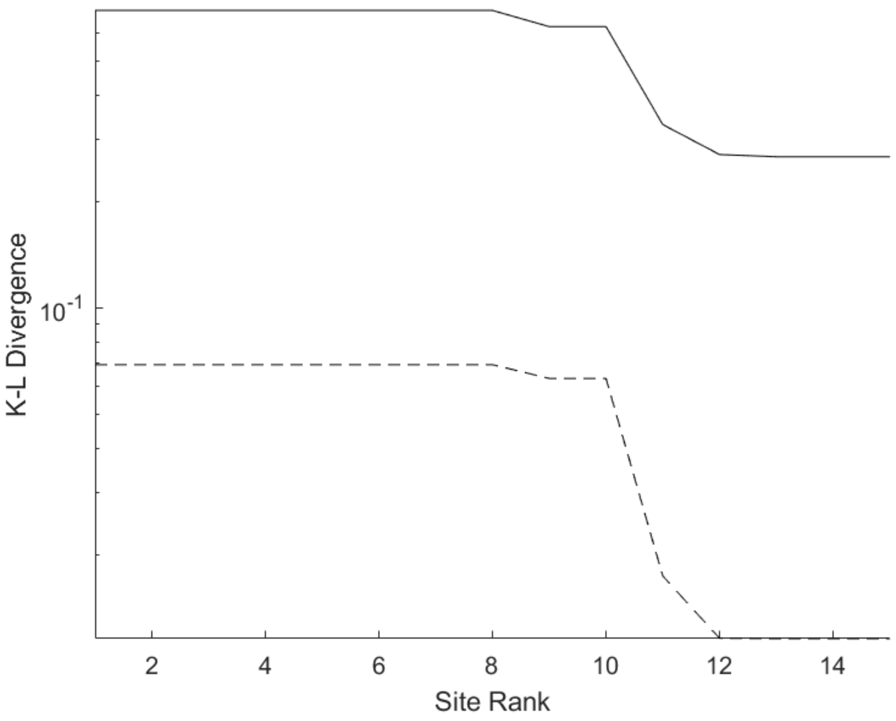

Partition 6, Late 2020, Oceania

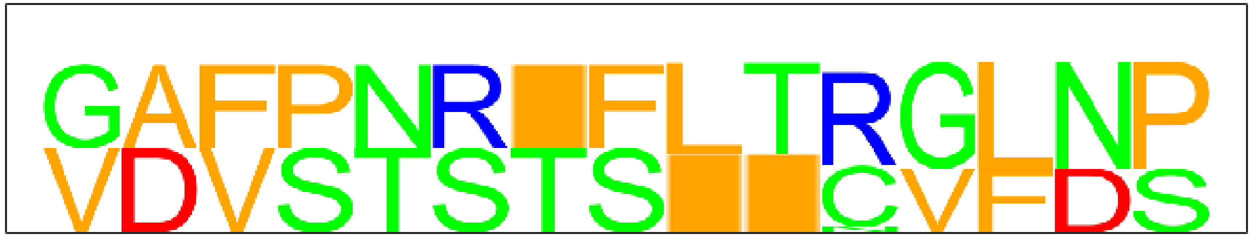

Partition 6, Oceania

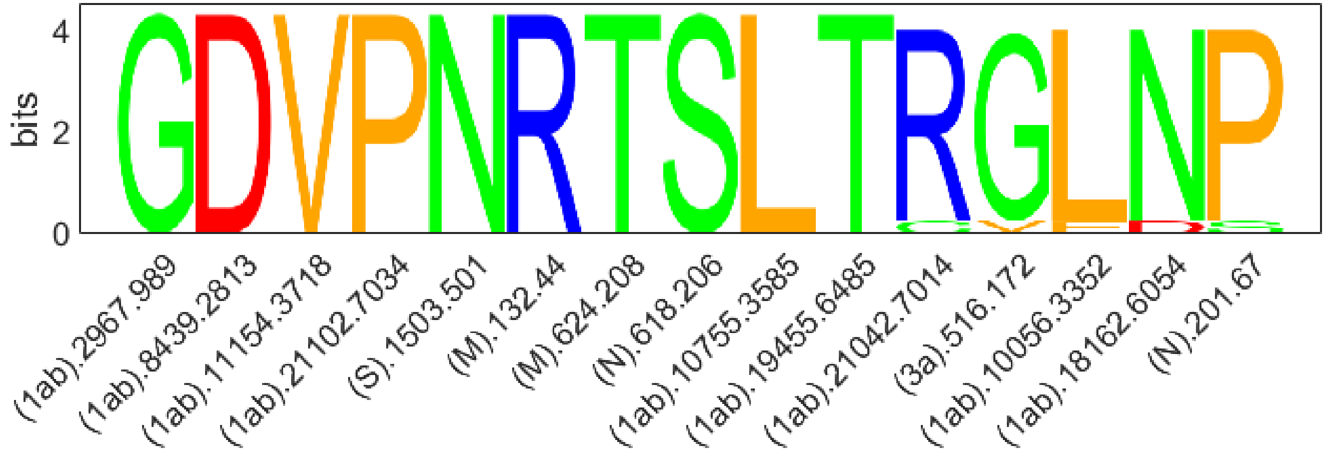

S21

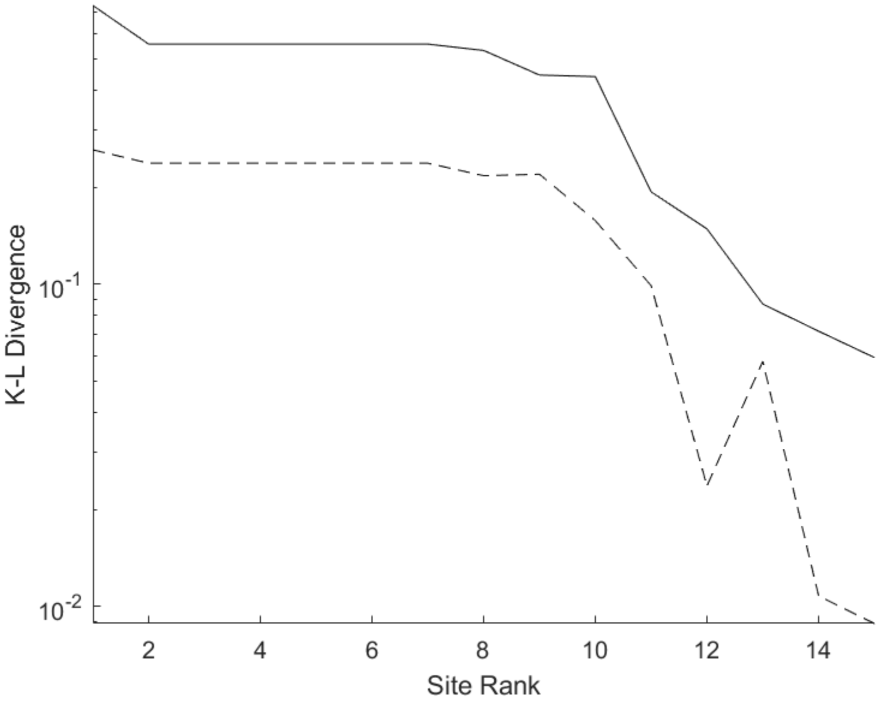

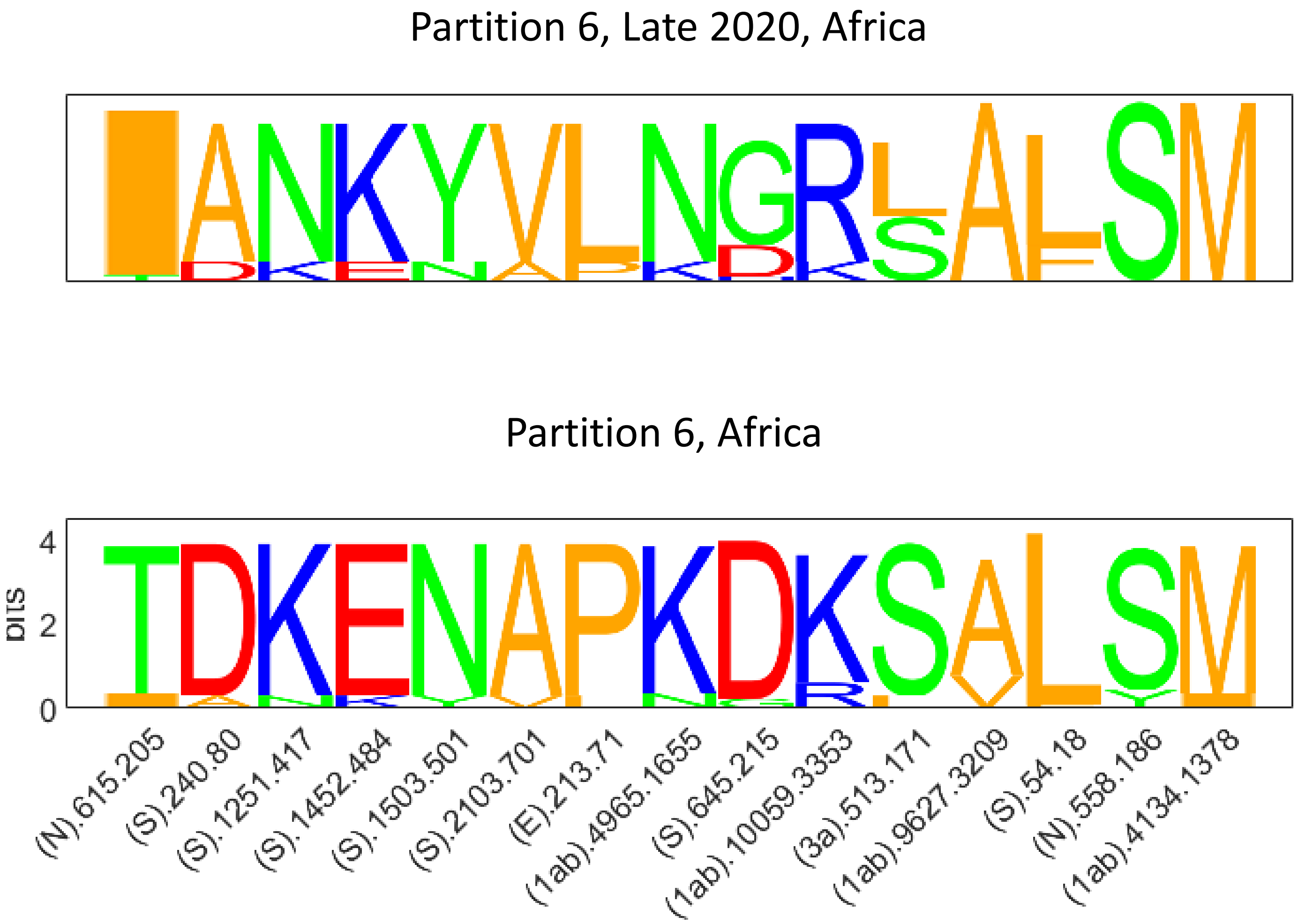
Partition 6, Late 2020, Africa

Partition 6, Africa

S22

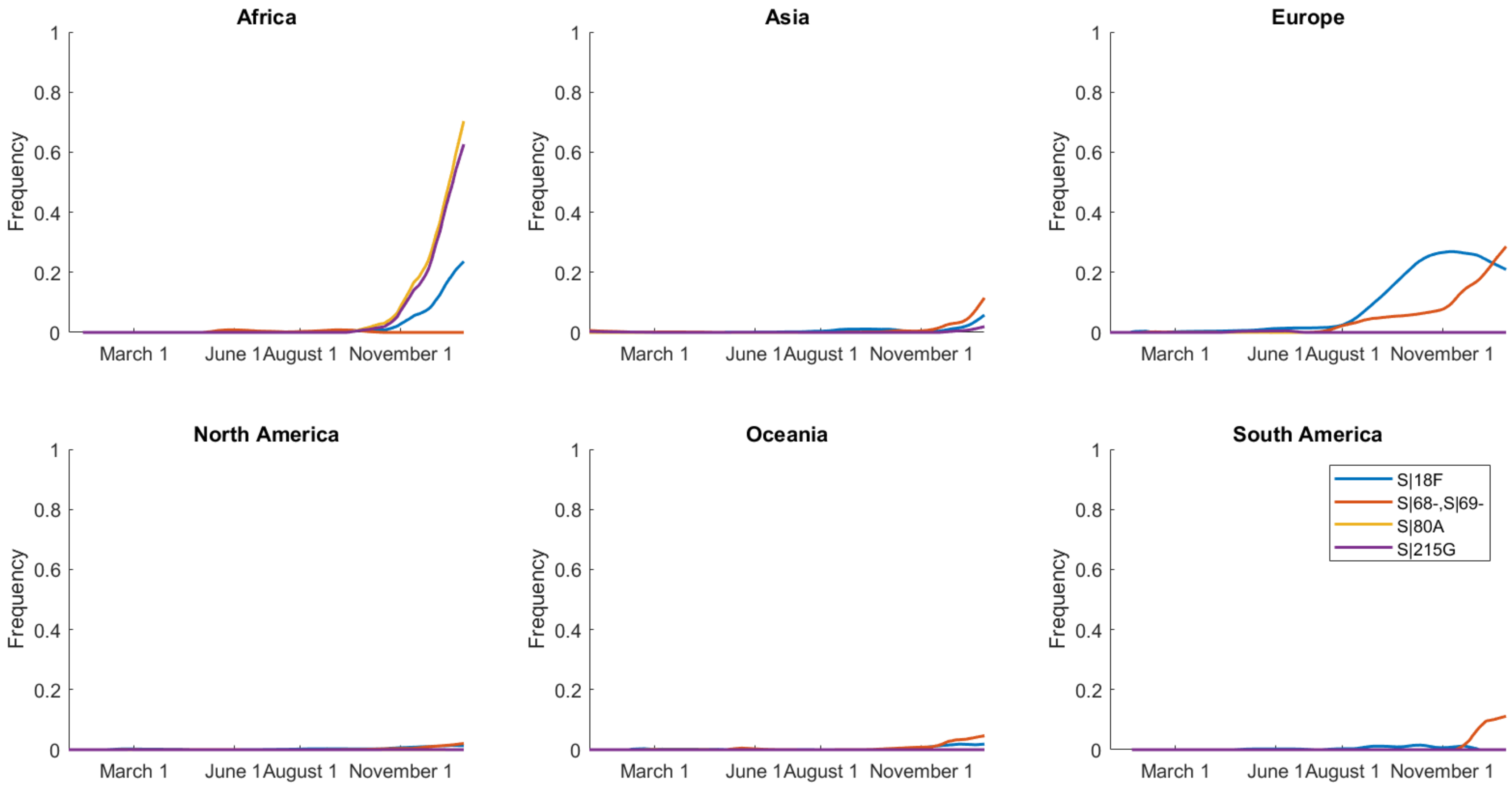
Africa
Asia
Europe
North America
Oceania
South America
Frequency
1
0.8
0.6
0.4
0.2
0
March 1
June 1
August 1
November 1
S|18F
S|68-,S|69-
S|80A
S|215G

S23

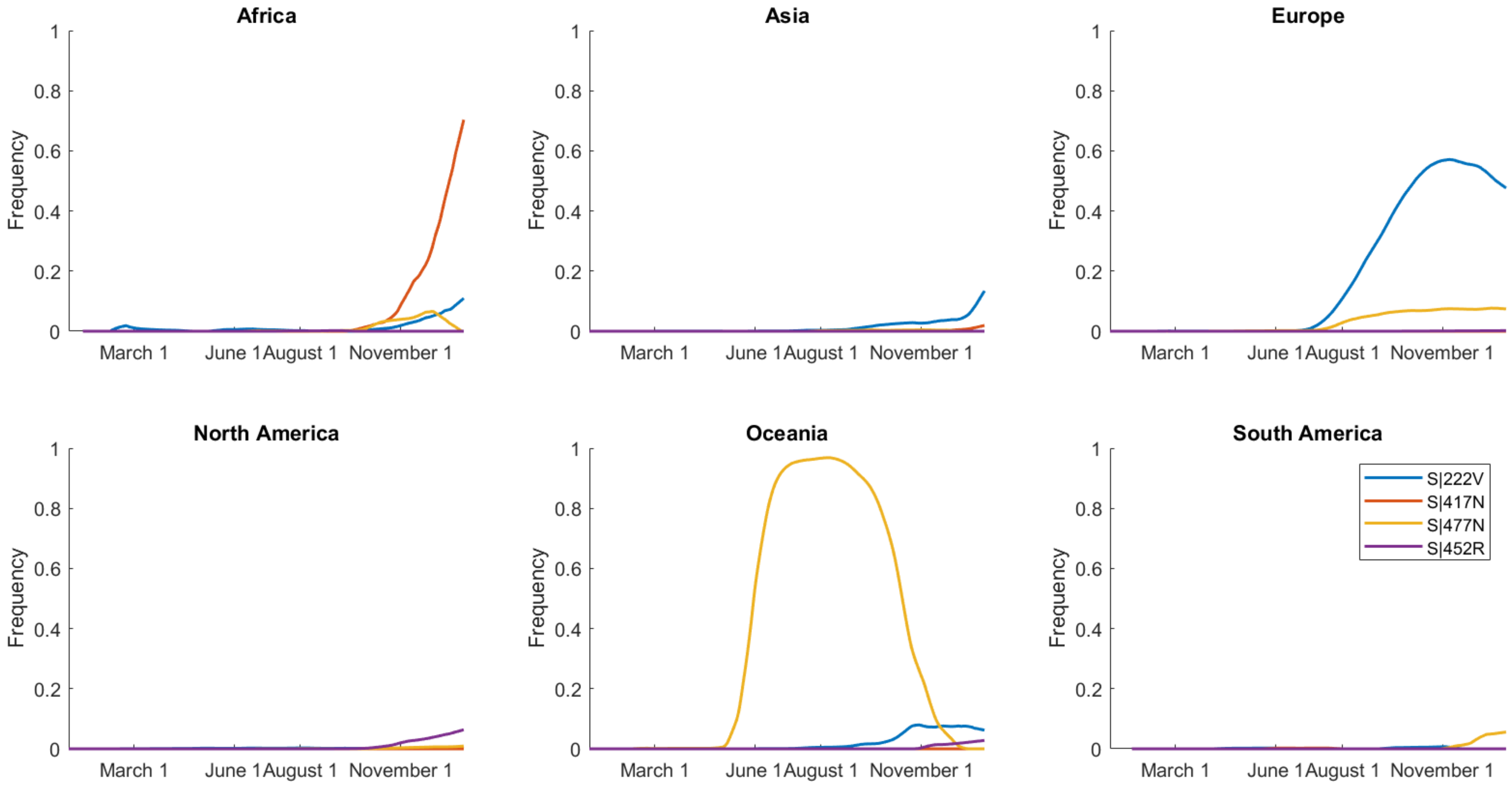
Africa
Asia
Europe
North America
Oceania
South America
Frequency
0
0.2
0.4
0.6
0.8
1
March 1
June 1
August 1
November 1
S|222V
S|417N
S|477N
S|452R

S24

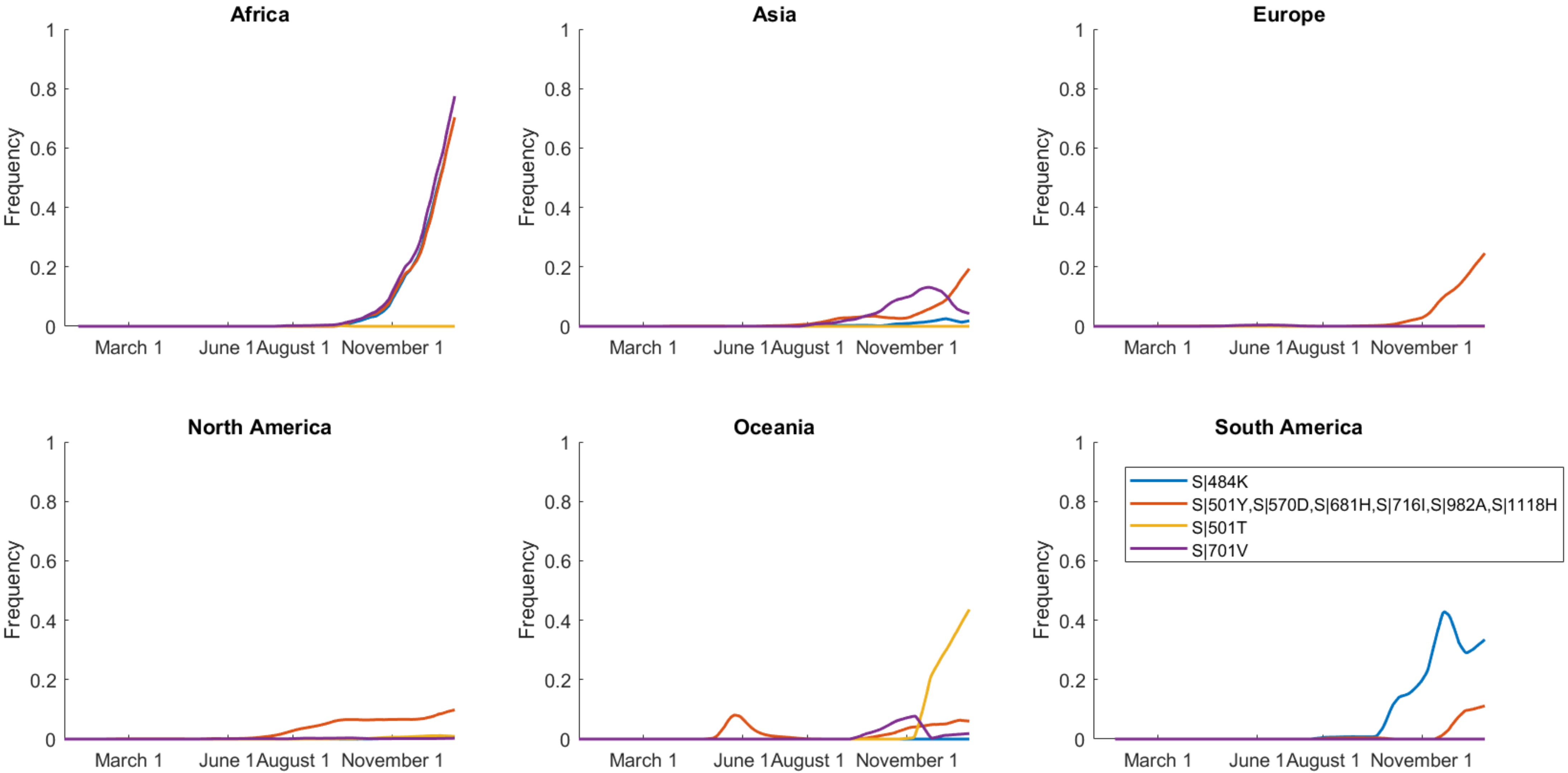
Africa
Asia
Europe
North America
Oceania
South America
Frequency
0
0.2
0.4
0.6
0.8
1
March 1
June 1
August 1
November 1
S|484K
S|501Y,S|570D,S|681H,S|716I,S|982A,S|1118H
S|501T
S|701V

S25

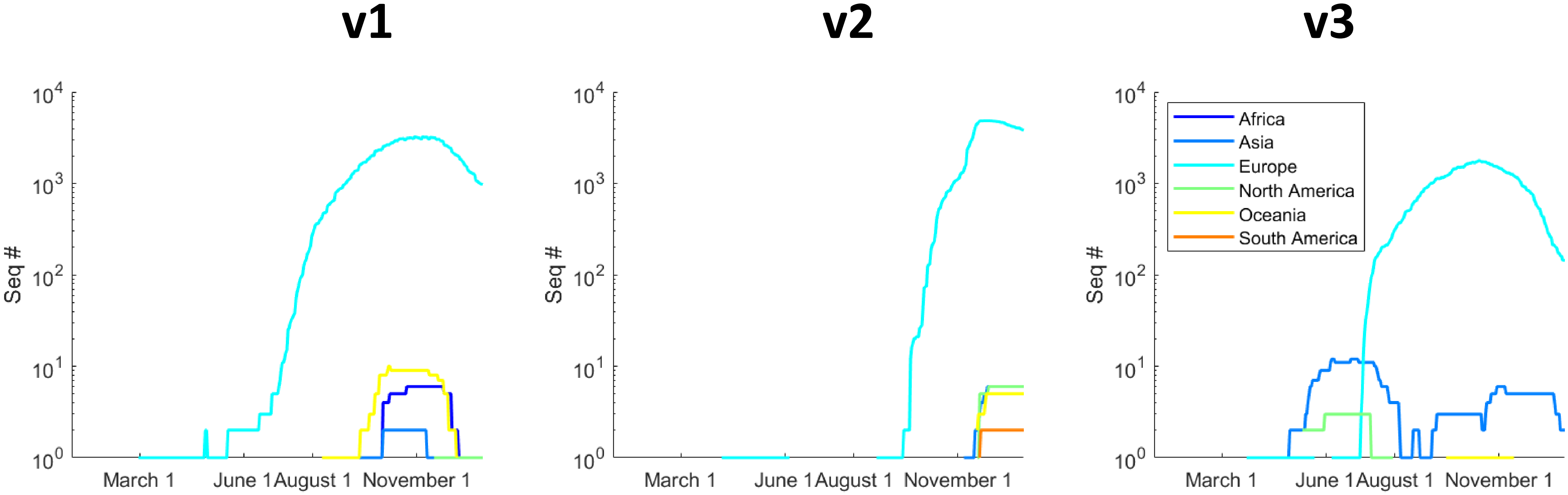
v1
v2
v3
Seq #
10^0
10^1
10^2
10^3
10^4
March 1
June 1
August 1
November 1
Africa
Asia
Europe
North America
Oceania
South America

Table S1

Location	Codon1	Codon2	Weight	#Events
orf1ab, 16	ctc(L)	ctt(L)	0.023	127
orf1ab, 24	cgc(R)	tgc(C)	0.004	85
orf1ab, 60	gtt(V)	gtc(V)	0.111	11
orf1ab, 140	cta(L)	tta(L)	0.003	87
orf1ab, 186	gtc(V)	gtt(V)	0.002	98
orf1ab, 265	acc(T)	atc(I)	0.131	71
orf1ab, 300	att(I)	ttt(F)	0.012	50
orf1ab, 309	cca(P)	cta(L)	0.003	96
orf1ab, 443	tcc(S)	ttc(F)	0.001	84
orf1ab, 473	atc(I)	att(I)	0.002	105
orf1ab, 519	ggt(G)	agt(S)	0.004	125
orf1ab, 540	gct(A)	gtt(V)	0.001	90
orf1ab, 549	tcc(S)	tct(S)	0.004	141
orf1ab, 717	tac(Y)	tat(Y)	0.017	20
orf1ab, 924	ttt(F)	ttc(F)	0.005	89
orf1ab, 924	ttc(F)	ttt(F)	0.784	20
orf1ab, 944	tca(S)	tta(L)	0.003	139
orf1ab,1113	cac(H)	tac(Y)	0.01	61
orf1ab,1246	act(T)	att(I)	0.011	29
orf1ab,1273	gac(D)	gat(D)	0.003	87
orf1ab,1426	acc(T)	act(T)	0.013	67
orf1ab,1627	cta(L)	tta(L)	0.003	91
orf1ab,1788	acg(T)	act(T)	0.012	28
orf1ab,1868	tac(Y)	tat(Y)	0.003	96
orf1ab,1925	ttc(F)	ttt(F)	0.004	88
orf1ab,2007	acc(T)	act(T)	0.111	46
orf1ab,2016	aca(T)	aaa(K)	0.012	13

orf1ab,2124	act(T)	att(I)	0.002	96
orf1ab,2221	ctt(L)	cct(P)	0.015	6
orf1ab,2226	ctg(L)	ttg(L)	0.009	25
orf1ab,2260	ctt(L)	cct(P)	0.041	3
orf1ab,2385	atc(I)	att(I)	0.002	85
orf1ab,2421	gtc(V)	gtt(V)	0.005	96
orf1ab,2501	atc(I)	acc(T)	0.012	11
orf1ab,2594	tac(Y)	tat(Y)	0.011	14
orf1ab,2839	agt(S)	agc(S)	0.893	21
orf1ab,2884	ttc(F)	ttt(F)	0.004	87
orf1ab,3055	atc(I)	att(I)	0.006	148
orf1ab,3076	cat(H)	tat(Y)	0.001	91
orf1ab,3087	atg(M)	att(I)	0.012	32
orf1ab,3143	gtt(V)	gct(A)	0.072	6
orf1ab,3278	ggt(G)	agt(S)	0.016	13
orf1ab,3291	aac(N)	aat(N)	0.002	101
orf1ab,3352	ctt(L)	ttt(F)	0.017	48
orf1ab,3353	aag(K)	agg(R)	0.01	226
orf1ab,3368	cgc(R)	cgt(R)	0.004	121
orf1ab,3535	ctg(L)	ctt(L)	0.008	89
orf1ab,3603	ttc(F)	ttt(F)	0.004	149
orf1ab,3606	ttt(F)	ttg(L)	0.008	107
orf1ab,3606	ttg(L)	ttt(F)	0.077	802
orf1ab,3655	atg(M)	att(I)	0.013	32
orf1ab,3690	gtg(V)	gtt(V)	0.001	86
orf1ab,3718	gtt(V)	ttt(F)	0.005	129
orf1ab,3744	tac(Y)	tat(Y)	0.011	18
orf1ab,3796	ctc(L)	ctt(L)	0.001	94
orf1ab,3884	tca(S)	tta(L)	0.013	55

orf1ab,4058	ccc(P)	cct(P)	0.002	88
orf1ab,4065	aca(T)	ata(I)	0.001	95
orf1ab,4083	acg(T)	atg(M)	0.002	85
orf1ab,4317	gag(E)	gat(D)	0.01	4
orf1ab,4424	tac(Y)	tat(Y)	0.012	66
orf1ab,4489	gct(A)	gtt(V)	0.014	46
orf1ab,4577	gct(A)	tct(S)	0.011	18
orf1ab,4619	cca(P)	cta(L)	0.002	85
orf1ab,4715	cct(P)	ctt(L)	0.785	26
orf1ab,4779	cta(L)	tta(L)	0.002	91
orf1ab,4820	ttc(F)	ttt(F)	0.003	121
orf1ab,4847	tac(Y)	tat(Y)	0.03	74
orf1ab,5020	aac(N)	aat(N)	0.034	91
orf1ab,5152	gac(D)	gat(D)	0.003	102
orf1ab,5158	ttc(F)	ttt(F)	0.003	104
orf1ab,5168	gtg(V)	ttg(L)	0.011	17
orf1ab,5214	cag(Q)	cat(H)	0.002	85
orf1ab,5541	tac(Y)	tat(Y)	0.007	257
orf1ab,5542	aaa(K)	aga(R)	0.011	4
orf1ab,5585	gag(E)	gat(D)	0.012	45
orf1ab,5614	cat(H)	tat(Y)	0.014	66
orf1ab,5680	gtc(V)	gtt(V)	0.001	93
orf1ab,5762	ctc(L)	ctt(L)	0.002	90
orf1ab,5828	ctt(L)	cct(P)	0.94	6
orf1ab,5865	tgt(C)	tat(Y)	0.939	1
orf1ab,5932	ctt(L)	ctc(L)	0.937	5
orf1ab,6054	aat(N)	gat(D)	0.011	11
orf1ab,6097	gac(D)	gat(D)	0.008	107
orf1ab,6205	cta(L)	tta(L)	0.048	77

orf1ab,6302	ttc(F)	ttt(F)	0.003	89
orf1ab,6335	aac(N)	aat(N)	0.002	91
orf1ab,6420	ctc(L)	ctt(L)	0.01	131
orf1ab,6525	aat(N)	aac(N)	0.013	58
orf1ab,6541	aag(K)	aaa(K)	0.893	1
orf1ab,6573	gtc(V)	gtt(V)	0.002	95
orf1ab,6579	gtt(V)	ttt(F)	0.001	86
orf1ab,6638	gtc(V)	gtt(V)	0.003	108
orf1ab,6668	tta(L)	ttg(L)	0.085	24
orf1ab,6958	aag(K)	agg(R)	0.005	197
orf1ab,6997	gcg(A)	gcc(A)	0.112	40
orf1ab,7014	cgc(R)	tgc(C)	0.011	30
S , 5 ctt(L)	ttt(F)	0.016	522	
S , 18	ctt(L)	ttt(F)	0.046	111
S , 22	act(T)	att(I)	0.002	85
S , 49	cat(H)	tat(Y)	0.003	89
S , 54	ttg(L)	ttt(F)	0.003	95
S , 95	act(T)	att(I)	0.003	105
S , 98	tct(S)	ttt(F)	0.011	78
S , 222	gct(A)	gtt(V)	0.114	81
S , 294	gac(D)	gat(D)	0.014	46
S , 439	aac(N)	aaa(K)	0.012	11
S , 475	gcc(A)	gct(A)	0.002	86
S , 477	agc(S)	aac(N)	0.013	41
S , 543	ttc(F)	ttt(F)	0.003	92
S , 614	gat(D)	ggt(G)	0.788	38
S , 614	ggt(G)	gat(D)	0.021	57
S , 677	cag(Q)	cat(H)	0.003	103
S , 723	acc(T)	act(T)	0.016	6

S , 769	gga(G)	gta(V)	0.003	88
S , 789	tac(Y)	tat(Y)	0.012	53
S , 821	cta(L)	tta(L)	0.002	89
S , 856	aac(N)	aat(N)	0.002	88
S , 924	gcc(A)	gct(A)	0.016	31
S , 939	tct(S)	ttt(F)	0.002	93
S ,1044	gga(G)	ggt(G)	0.009	8
orf3a , 13	gta(V)	tta(L)	0.01	57
orf3a , 38	caa(Q)	cga(R)	0.009	9
orf3a , 43	ttc(F)	ttt(F)	0.003	115
orf3a , 57	cag(Q)	cat(H)	0.203	70
orf3a , 64	atc(I)	acc(T)	0.041	3
orf3a , 78	cac(H)	tac(Y)	0.002	86
orf3a , 106	ctc(L)	ttc(F)	0.001	86
orf3a , 106	ctc(L)	ctt(L)	0.013	73
orf3a , 131	tgg(W)	tgt(C)	0.003	97
orf3a , 151	act(T)	att(I)	0.002	97
orf3a , 155	gac(D)	tac(Y)	0.002	87
orf3a , 171	tca(S)	tta(L)	0.004	126
orf3a , 172	ggt(G)	cgt(R)	0.009	12
orf3a , 172	ggt(G)	gtt(V)	0.012	37
orf3a , 175	aca(T)	ata(I)	0.004	93
orf3a , 202	gta(V)	tta(L)	0.01	52
orf3a , 232	att(I)	atc(I)	0.919	7
orf3a , 251	ggt(G)	gtt(V)	0.023	13
E , 4 ttc(F)	ttt(F)	0.001	86	
E , 73	ctt(L)	ttt(F)	0.002	93
M , 3	gat(D)	ggt(G)	0.009	23
M , 41	aac(N)	aat(N)	0.002	86

M	, 53	ttc(F)	ttt(F)	0.006	175
M	, 71	tac(Y)	tat(Y)	0.035	107
M	, 93	ctc(L)	ctt(L)	0.003	96
M	, 93	ctc(L)	ctg(L)	0.111	8
M	, 117	aac(N)	aat(N)	0.001	98
M	, 118	att(I)	atc(I)	0.011	11
M	, 125	cat(H)	tat(Y)	0.003	97
orf6	, 4	ctc(L)	ctt(L)	0.003	103
orf6	, 32	atc(I)	att(I)	0.001	90
orf6	, 61	gat(D)	gac(D)	0.006	169
orf7b	, 15	gcc(A)	gca(A)	0.009	6
orf8	, 17	cat(H)	cac(H)	0.039	15
orf8	, 17	cac(H)	cat(H)	0.073	49
orf8	, 24	tca(S)	tta(L)	0.027	38
orf8	, 62	gtg(V)	ttg(L)	0.005	157
orf8	, 65	gct(A)	gtt(V)	0.005	122
orf8	, 67	tct(S)	ttt(F)	0.003	138
orf8	, 84	tca(S)	tta(L)	0.891	8
orf8	, 120	ttc(F)	ttt(F)	0.007	236
N	, 13	ccc(P)	ctc(L)	0.015	78
N	, 35	gcg(A)	gct(A)	0.004	101
N	, 67	cct(P)	tct(S)	0.011	30
N	, 110	ttc(F)	ttt(F)	0.003	118
N	, 126	aac(N)	aat(N)	0.01	40
N	, 128	gac(D)	gat(D)	0.009	89
N	, 139	ttt(F)	ttg(L)	0.085	2
N	, 192	aac(N)	aat(N)	0.002	88
N	, 193	agt(S)	att(I)	0.004	88
N	, 194	tca(S)	tta(L)	0.065	131

N	, 199	cca(P)	cta(L)	0.021	35
N	, 202	agt(S)	aat(N)	0.018	14
N	, 203	agg(R)	aag(K)	0.254	29
N	, 203	aag(K)	aaa(K)	0.252	1
N	, 204	gga(G)	cga(R)	0.251	10
N	, 205	act(T)	att(I)	0.009	123
N	, 220	gct(A)	gtt(V)	0.112	21
N	, 234	atg(M)	att(I)	0.006	93
N	, 234	atg(M)	atc(I)	0.011	10
N	, 274	ttt(F)	ttc(F)	0.886	6
N	, 274	ttc(F)	ttt(F)	0.009	159
N	, 327	tcg(S)	ttg(L)	0.001	89
N	, 365	cca(P)	tca(S)	0.01	37
N	, 376	gct(A)	act(T)	0.011	8
N	, 377	gat(D)	tat(Y)	0.007	148

Table S2

List 1, unrestricted by single substitution weight

Location	Codon1	Codon2	Weight	#Events
S , 614	gat(D)	ggt(G)	0.788	38
N , 203	agg(R)	aag(K)	0.254	29
N , 204	gga(G)	cga(R)	0.251	10
orf3a , 57	cag(Q)	cat(H)	0.203	70
orf1ab,3606	ttg(L)	ttt(F)	0.077	802
orf3a , 251	ggt(G)	gtt(V)	0.023	13
S , 614	ggt(G)	gat(D)	0.021	57
N , 202	agt(S)	aat(N)	0.018	14
orf1ab,3278	ggt(G)	agt(S)	0.016	13
S , 477	agc(S)	aac(N)	0.013	41
orf1ab,3655	atg(M)	att(I)	0.013	32
orf1ab, 300	att(I)	ttt(F)	0.012	50
orf1ab,5585	gag(E)	gat(D)	0.012	45
orf1ab,3087	atg(M)	att(I)	0.012	32
orf3a , 172	ggt(G)	gtt(V)	0.012	37
orf1ab,2501	atc(I)	acc(T)	0.012	11
orf1ab,5168	gtg(V)	ttg(L)	0.011	17
orf1ab,4577	gct(A)	tct(S)	0.011	18
orf1ab,6054	aat(N)	gat(D)	0.011	11
N , 376	gct(A)	act(T)	0.011	8
N , 234	atg(M)	atc(I)	0.011	10
orf3a , 13	gta(V)	tta(L)	0.01	57
orf3a , 202	gta(V)	tta(L)	0.01	52
orf1ab,3353	aag(K)	agg(R)	0.01	226
orf3a , 172	ggt(G)	cgt(R)	0.009	12

orf3a , 38	caa(Q)	cga(R)	0.009	9
M , 3	gat(D)	ggt(G)	0.009	23
orf1ab,3606	ttt(F)	ttg(L)	0.008	107
N , 194	tta(L)	tca(S)	0.008	29
S , 262	gct(A)	tct(S)	0.008	38
orf8 , 92	gaa(E)	aaa(K)	0.007	9
orf1ab,5922	gca(A)	tca(S)	0.007	21
N , 377	gat(D)	tat(Y)	0.007	148
orf1ab,4241	atg(M)	att(I)	0.007	10
orf1ab,2702	cag(Q)	cat(H)	0.007	27
N , 292	atc(I)	acc(T)	0.007	13
orf6 , 33	ata(I)	aca(T)	0.006	12
orf3a , 75	aag(K)	aat(N)	0.006	26
orf1ab,5048	gct(A)	tct(S)	0.006	40
N , 234	atg(M)	att(I)	0.006	93
orf1ab,3334	ggt(G)	agt(S)	0.006	23
orf8 , 62	gtg(V)	ctg(L)	0.006	18
orf3a , 196	gga(G)	gta(V)	0.006	8
orf8 , 52	aga(R)	ata(I)	0.005	31
S , 501	aat(N)	tat(Y)	0.005	8
orf1ab,6958	aag(K)	agg(R)	0.005	197
orf1ab,3934	atg(M)	att(I)	0.005	37
orf8 , 62	gtg(V)	ttg(L)	0.005	157
N , 103	gat(D)	tat(Y)	0.005	25
orf1ab,3718	gtt(V)	ttt(F)	0.005	129
orf1ab,2606	atg(M)	ata(I)	0.005	9
S ,1176	gtt(V)	ttt(F)	0.005	52
orf1ab,3839	aaa(K)	aga(R)	0.004	9
orf1ab, 519	ggt(G)	agt(S)	0.004	125

orf1ab,1202	aag(K)	aat(N)	0.004	58
orf1ab, 315	atg(M)	att(I)	0.004	9
orf1ab,2873	ata(I)	aca(T)	0.004	20
orf1ab,3353	agg(R)	aag(K)	0.004	9
N , 193	agt(S)	att(I)	0.004	88
orf1ab,3712	atg(M)	att(I)	0.003	12
S ,1163	gat(D)	tat(Y)	0.003	54
N , 209	aga(R)	ata(I)	0.003	70
orf1ab,4653	tta(L)	tgc(C)	0.003	39
orf1ab,6426	atg(M)	att(I)	0.003	34
orf1ab, 379	gga(G)	gaa(E)	0.003	29
S , 54	ttg(L)	ttt(F)	0.003	95
S , 153	atg(M)	acg(T)	0.003	45
S , 677	cag(Q)	cat(H)	0.003	103
S , 583	gag(E)	gat(D)	0.003	73
S , 583	gag(E)	gac(D)	0.003	13
orf1ab,4080	tat(Y)	cat(H)	0.003	25
S , 21	aga(R)	ata(I)	0.003	49
orf1ab,1247	aag(K)	aat(N)	0.003	16
S , 80	gat(D)	tat(Y)	0.003	59
orf3a , 131	tgg(W)	tgt(C)	0.003	97
S , 769	gga(G)	gta(V)	0.003	88
orf1ab,1655	aag(K)	aat(N)	0.002	47
orf1ab,5058	atg(M)	att(I)	0.002	29
orf1ab,2796	atg(M)	att(I)	0.002	19
orf1ab, 190	ttc(F)	ctc(L)	0.002	13
orf1ab,5568	gag(E)	gat(D)	0.002	18
S ,1078	gct(A)	tct(S)	0.002	84
orf3a , 224	ggt(G)	tgt(C)	0.002	82

orf1ab,5784	aag(K)	agg(R)	0.002	26
orf8 , 65	gct(A)	tct(S)	0.002	67
N , 180	agt(S)	att(I)	0.002	60
N , 190	agt(S)	att(I)	0.002	11
orf1ab,4715	ctt(L)	cct(P)	0.002	67
orf1ab, 673	gag(E)	aag(K)	0.002	10
orf1ab,4646	gag(E)	gat(D)	0.002	9
orf3a , 122	aga(R)	ata(I)	0.002	15
S ,1167	ggt(G)	gtt(V)	0.002	14
orf8 , 84	tta(L)	tca(S)	0.002	23
orf1ab,5620	gct(A)	tct(S)	0.002	62
S , 839	gat(D)	tat(Y)	0.002	33
orf1ab,6826	caa(Q)	cac(H)	0.002	18

List 2, restricted by single substitution weight

S , 614	gat(D)	ggt(G)	0.788	38
N , 203	agg(R)	aag(K)	0.254	29
N , 204	gga(G)	cga(R)	0.251	10
orf3a , 57	cag(Q)	cat(H)	0.203	70
orf3a , 251	ggt(G)	gtt(V)	0.023	13
N , 202	agt(S)	aat(N)	0.018	14
orf1ab,3278	ggt(G)	agt(S)	0.016	13
orf1ab,2501	atc(I)	acc(T)	0.012	11
orf1ab,5168	gtg(V)	ttg(L)	0.011	17
orf1ab,4577	gct(A)	tct(S)	0.011	18
orf1ab,6054	aat(N)	gat(D)	0.011	11
N , 376	gct(A)	act(T)	0.011	8
N , 234	atg(M)	atc(I)	0.011	10
orf3a , 172	ggt(G)	cgt(R)	0.009	12

orf3a , 38	caa(Q)	cga(R)	0.009	9
orf8 , 92	gaa(E)	aaa(K)	0.007	9
orf1ab,4241	atg(M)	att(I)	0.007	10
N , 292	atc(I)	acc(T)	0.007	13
orf6 , 33	ata(I)	aca(T)	0.006	12
orf3a , 196	gga(G)	gta(V)	0.006	8
S , 501	aat(N)	tat(Y)	0.005	8
orf1ab,2606	atg(M)	ata(I)	0.005	9

Table S3

state 1	state 2	#simultaneous,	#1Follows2,	#2Follows1,	#1alone,	#2alone,	Poisson Score,	Binomial Score
orf1ab|N6054D	orf3a|G172V	8	1	0	2	29	4.500297	54.71266
N|M234I	N|A376T	6	0	0	4	2	4.570825	45.70371
orf3a|G172R	orf3a|V202L	6	0	1	6	45	4.71351	35.39944
orf3a|Q38R	orf3a|G172R	5	1	0	3	7	4.716511	40.63884
orf3a|Q38R	orf3a|V202L	4	1	1	4	47	4.713664	27.3363
orf1ab|A4577S	orf1ab|V5168L	4	0	0	14	13	4.507175	20.22504
orf6|I33T	N|I292T	3	2	0	7	10	5.094976	28.08009
orf3a|Q57H	N|A376T	3	0	5	67	0	4.507881	15.89292
orf1ab|M3087I	N|M234I	3	0	0	29	7	4.576141	13.96507
orf1ab|V5168L	orf1ab|E5585D	3	0	1	14	41	4.508892	13.21509
orf1ab|A4577S	orf1ab|E5585D	3	0	1	15	41	4.510709	13.05832
orf1ab|M3087I	S|S477N	3	1	0	28	38	4.512101	11.51581
orf1ab|F3606L	orf3a|G251V	2	8	2	97	9	6.000492	21.155
orf1ab|V5168L	N|A376T	2	0	2	15	4	4.516232	17.86805
orf1ab|A4577S	N|A376T	2	0	2	16	4	4.515504	17.77572
orf1ab|V5168L	N|M234I	2	0	2	15	6	4.573518	16.88806
orf1ab|A4577S	N|M234I	2	0	2	16	6	4.572747	16.79526
orf1ab|E5585D	N|A376T	2	0	2	43	4	4.516768	15.89794
S|S477N	N|A376T	2	0	2	39	4	4.518391	15.71228
orf1ab|M3087I	N|A376T	2	0	1	30	5	4.518707	12.344
orf1ab|M3087I	orf1ab|V5168L	2	2	0	28	15	4.508153	11.72508
orf1ab|M3087I	orf1ab|A4577S	2	2	0	28	16	4.509245	11.63222
orf3a|Q57H	N|M234I	2	0	6	68	2	4.566414	11.12497
orf1ab|V5168L	S|S477N	2	1	1	14	38	4.51357	11.08201
orf1ab|E5585D	N|M234I	2	0	1	43	7	4.580214	11.05084
S|S477N	N|M234I	2	0	1	39	7	4.581944	10.9561
orf1ab|A4577S	S|S477N	2	1	1	15	38	4.514669	10.92172

orf1ab|E5585D	S|S477N	2	1	1	42	38	4.514105	8.188651
orf1ab|M3087I	orf1ab|E5585D	2	1	0	29	43	4.51442	7.328134
orf1ab|M2606I	N|D377Y	1	1	7	7	140	6.263857	20.83678
orf3a|G172V	N|D377Y	1	0	12	36	135	6.238693	18.84826
S|L54F	N|G204R	1	46	0	48	9	6.73894	18.65395
S|D614G	S|G769V	1	0	84	37	3	6.021858	15.57247
orf1ab|V3718F	S|D614G	1	120	0	8	37	5.52613	14.76006
orf1ab|M3655I	orf3a|K75N	1	3	0	28	25	5.519532	11.20034
N|G204R	N|D377Y	1	0	54	9	93	6.29775	9.879498
orf3a|Q57H	N|D377Y	1	0	44	69	103	5.656636	6.994133
S|D614G	orf8|R52I	1	0	29	37	1	5.266064	6.870319
orf1ab|E4646D	orf1ab|M6426I	1	0	0	8	33	6.198232	6.284282
S|D1163Y	S|G1167V	1	0	0	53	13	6.341247	5.391188
orf1ab|I2873T	orf1ab|L4653C	0	4	9	16	30	6.259714	45.86258
orf1ab|K3353R	orf1ab|R3353K	0	2	9	224	0	5.610998	43.42658
S|M153T	N|G204R	0	35	0	10	10	5.958639	29.31147
S|M153T	N|R203K	0	35	0	10	29	5.958639	28.9565
orf1ab|Y4080H	N|G204R	0	22	0	3	10	5.938512	23.50665
orf1ab|Y4080H	N|R203K	0	22	0	3	29	5.933536	23.27143
orf1ab|K6958R	S|D614G	0	187	0	10	38	5.402686	22.38333
orf8|V62L	N|G204R	0	73	0	84	10	6.119245	19.05969
orf1ab|K3353R	N|R203K	0	97	0	129	29	5.892221	18.77014
orf1ab|K3353R	N|G204R	0	96	0	130	10	5.90064	18.56422
orf8|V62L	N|R203K	0	73	0	84	29	6.119245	18.55167
S|D614G	orf8|V62L	0	0	149	38	8	5.449372	18.05377
S|D614G	N|D377Y	0	0	141	38	7	5.034589	17.96663
orf1ab|F190L	orf3a|Q57H	0	12	0	1	70	6.03815	16.77026
S|D614G	S|Q677H	0	0	100	38	3	5.935846	16.30013
S|L54F	N|R203K	0	46	1	49	28	6.742405	16.20734

orf1ab|N6054D	N|D377Y	0	0	12	11	136	6.245713	15.72337
orf3a|K75N	N|G204R	0	19	0	7	10	5.106553	14.77935
S|L54F	S|D614G	0	92	0	3	38	5.861692	14.62789
orf3a|K75N	N|R203K	0	19	0	7	29	5.105208	14.59149
S|D614G	S|A1078S	0	0	82	38	2	6.09119	14.40707
S|E583D	S|D614G	0	71	1	2	37	5.937666	14.33601
orf1ab|G3334S	N|G204R	0	17	0	6	10	5.263173	13.60533
orf1ab|G3334S	N|R203K	0	17	0	6	29	5.263173	13.43616
orf1ab|M2606I	orf1ab|N6054D	0	4	0	5	11	5.400463	13.152
orf1ab|M2606I	orf3a|G172V	0	4	0	5	37	5.408572	12.98435
orf1ab|G519S	N|R203K	0	55	0	70	29	6.321092	12.28335
orf1ab|G519S	N|G204R	0	54	0	71	10	6.323203	11.78333
orf1ab|R3353K	S|N501Y	0	3	0	6	8	5.660511	11.4252
orf1ab|R3353K	orf8|R52I	0	3	0	6	31	5.660511	11.36166
orf1ab|K6958R	N|R203K	0	77	0	120	29	6.282133	11.04242
orf1ab|K1202N	S|D614G	0	57	0	1	38	5.513131	11.01896
orf1ab|K6958R	N|G204R	0	76	0	121	10	6.291696	10.80214
S|G769V	N|R203K	0	40	0	48	29	6.67367	10.25443
orf1ab|A5620S	S|D614G	0	60	0	2	38	6.260371	9.741035
S|G769V	N|G204R	0	39	0	49	10	6.689564	9.610466
S|D614G	N|M234I	0	0	87	38	6	5.19501	9.320778
orf1ab|R3353K	orf1ab|K5784R	0	0	3	9	23	6.414769	9.035853
orf1ab|L4715P	S|D614G	0	64	0	3	38	6.133894	8.959117
S|D614G	orf3a|G224C	0	0	77	38	5	6.170657	8.735977
S|D614G	orf3a|W131C	0	0	90	38	7	6.142963	8.720943
orf1ab|K1655N	S|D614G	0	46	0	1	38	6.019098	8.592451
orf3a|Q57H	N|M234I	0	0	34	70	59	6.360114	8.447752
orf1ab|L4653C	orf3a|Q57H	0	18	0	21	70	6.545867	8.285261
S|D614G	S|D1163Y	0	0	52	38	2	5.833373	8.094074

<table>
<tr><th></th><th></th><th></th><th></th><th></th><th></th><th></th><th></th><th></th></tr>
<tr><td>orf1ab|K5784R</td><td>S|N501Y</td><td>0</td><td>3</td><td>0</td><td>23</td><td>8</td><td>6.411709</td><td>8.057716</td></tr>
<tr><td>orf1ab|K5784R</td><td>orf8|R52I</td><td>0</td><td>3</td><td>0</td><td>23</td><td>31</td><td>6.411709</td><td>7.995575</td></tr>
<tr><td>orf1ab|M3655I</td><td>orf1ab|M3712I</td><td>0</td><td>0</td><td>3</td><td>32</td><td>9</td><td>5.803803</td><td>7.827436</td></tr>
<tr><td>orf1ab|M3934I</td><td>N|G204R</td><td>0</td><td>19</td><td>0</td><td>18</td><td>10</td><td>5.430497</td><td>7.536757</td></tr>
<tr><td>S|D80Y</td><td>S|D614G</td><td>0</td><td>56</td><td>0</td><td>3</td><td>38</td><td>6.053853</td><td>7.414205</td></tr>
<tr><td>orf1ab|M3934I</td><td>N|R203K</td><td>0</td><td>19</td><td>0</td><td>18</td><td>29</td><td>5.413549</td><td>7.386413</td></tr>
<tr><td>S|R21I</td><td>N|G204R</td><td>0</td><td>23</td><td>0</td><td>26</td><td>10</td><td>6.15872</td><td>7.189978</td></tr>
<tr><td>S|V1176F</td><td>N|G204R</td><td>0</td><td>24</td><td>0</td><td>28</td><td>10</td><td>5.6205</td><td>7.14312</td></tr>
<tr><td>S|R21I</td><td>S|D614G</td><td>0</td><td>47</td><td>0</td><td>2</td><td>38</td><td>5.963357</td><td>7.083728</td></tr>
<tr><td>S|R21I</td><td>N|R203K</td><td>0</td><td>23</td><td>0</td><td>26</td><td>29</td><td>6.15872</td><td>7.023278</td></tr>
<tr><td>S|V1176F</td><td>N|R203K</td><td>0</td><td>24</td><td>0</td><td>28</td><td>29</td><td>5.61286</td><td>6.972379</td></tr>
<tr><td>orf1ab|M5058I</td><td>S|D614G</td><td>0</td><td>29</td><td>0</td><td>0</td><td>38</td><td>6.018445</td><td>6.914705</td></tr>
<tr><td>N|R203K</td><td>N|D377Y</td><td>0</td><td>0</td><td>55</td><td>29</td><td>93</td><td>6.29775</td><td>6.904404</td></tr>
<tr><td>N|G204R</td><td>N|I292T</td><td>0</td><td>0</td><td>9</td><td>10</td><td>4</td><td>5.048052</td><td>6.892418</td></tr>
<tr><td>orf1ab|L4653C</td><td>S|D614G</td><td>0</td><td>38</td><td>0</td><td>1</td><td>38</td><td>5.802561</td><td>6.856622</td></tr>
<tr><td>N|R203K</td><td>N|I292T</td><td>0</td><td>0</td><td>9</td><td>29</td><td>4</td><td>5.048052</td><td>6.804806</td></tr>
<tr><td>orf1ab|G519S</td><td>S|D614G</td><td>0</td><td>112</td><td>0</td><td>13</td><td>38</td><td>5.70681</td><td>6.772864</td></tr>
<tr><td>orf1ab|R3353K</td><td>N|G204R</td><td>0</td><td>7</td><td>0</td><td>2</td><td>10</td><td>5.627283</td><td>6.591458</td></tr>
<tr><td>orf1ab|E4646D</td><td>N|G204R</td><td>0</td><td>7</td><td>0</td><td>2</td><td>10</td><td>6.16426</td><td>6.591458</td></tr>
<tr><td>orf1ab|E4646D</td><td>N|R203K</td><td>0</td><td>7</td><td>0</td><td>2</td><td>29</td><td>6.16426</td><td>6.51952</td></tr>
<tr><td>orf1ab|R3353K</td><td>N|R203K</td><td>0</td><td>7</td><td>0</td><td>2</td><td>29</td><td>5.627283</td><td>6.51952</td></tr>
<tr><td>S|M153T</td><td>S|D614G</td><td>0</td><td>43</td><td>0</td><td>2</td><td>38</td><td>5.882746</td><td>6.288292</td></tr>
<tr><td>S|E583D</td><td>N|G204R</td><td>0</td><td>30</td><td>0</td><td>43</td><td>10</td><td>6.588477</td><td>6.238237</td></tr>
<tr><td>orf1ab|K5784R</td><td>S|D614G</td><td>0</td><td>26</td><td>0</td><td>0</td><td>38</td><td>6.045193</td><td>6.199391</td></tr>
<tr><td>S|D614G</td><td>orf3a|K75N</td><td>0</td><td>0</td><td>26</td><td>38</td><td>0</td><td>5.072081</td><td>6.199391</td></tr>
<tr><td>S|D614G</td><td>S|V1176F</td><td>0</td><td>0</td><td>49</td><td>38</td><td>3</td><td>5.420556</td><td>6.10242</td></tr>
<tr><td>S|E583D</td><td>N|R203K</td><td>0</td><td>30</td><td>0</td><td>43</td><td>29</td><td>6.588477</td><td>6.053632</td></tr>
<tr><td>orf1ab|M3712I</td><td>orf3a|K75N</td><td>0</td><td>2</td><td>0</td><td>10</td><td>26</td><td>5.806855</td><td>5.990137</td></tr>
<tr><td>orf1ab|Y4080H</td><td>S|D614G</td><td>0</td><td>25</td><td>0</td><td>0</td><td>38</td><td>5.893439</td><td>5.960952</td></tr>
</table>

orf1ab|Q2702H	orf3a|Q57H	0	12	0	15	70	5.166565	5.533389
S|N501Y	N|G204R	0	6	0	2	10	5.327998	5.448073
orf3a|Q57H	N|R209I	0	0	24	70	46	6.823591	5.402
S|N501Y	N|R203K	0	6	0	2	29	5.327998	5.387137
orf1ab|I300F	orf1ab|E4646D	0	0	2	50	7	6.191473	5.314163
orf1ab|A5048S	S|D614G	0	38	0	2	38	5.097618	5.31327

Table S4

List 1

Variant_Mutation	Variant_ID
S|N501Y	B.1.1.7,B.1.1.7_E484K,B.1.351,P.1,v2,vAfrica
S|D614G	B.1.1.7,B.1.1.7_E484K,B.1.351,P.1,P.2
S|E484K	B.1.1.7_E484K,B.1.351,P.1,P.2,vAfrica
DELETION_ORF1A(NSP6)_3675-3677	B.1.1.7,B.1.1.7_E484K,B.1.351,P.1
S|A570D	B.1.1.7,B.1.1.7_E484K,v2,v3
N|D3L	B.1.1.7,B.1.1.7_E484K,v2
N|S235F	B.1.1.7,B.1.1.7_E484K,v2
S|D1118H	B.1.1.7,B.1.1.7_E484K,v2
S|H69-	B.1.1.7,B.1.1.7_E484K,B.1.258_DELTA
S|L18F	B.1.351,P.1,vAfrica
S|P681H	B.1.1.7,B.1.1.7_E484K,v2
S|S982A	B.1.1.7,B.1.1.7_E484K,v2
S|T716I	B.1.1.7,B.1.1.7_E484K,v2
S|V70-	B.1.1.7,B.1.1.7_E484K,B.1.258_DELTA
N|M234I	P.2,v1
N|T205I	B.1.351,vAfrica
ORF8|Q27*	B.1.1.7,B.1.1.7_E484K
S|A701V	B.1.351,vAfrica
S|D215G	B.1.351,vAfrica
S|D80A	B.1.351,vAfrica
S|K417N	B.1.351,vAfrica
S|Y144-	B.1.1.7,B.1.1.7_E484K
DELETION_S_242-245	B.1.351
E|P71L	vAfrica
M|R44S	vOceania

M|T208I	vOceania
NSP12|V720I	B.1.258_DELTA
NSP13|A598S	B.1.258_DELTA
NSP9|M101I	B.1.258_DELTA
N|A119S	P.2
N|A376T	v1
N|A398V	v3
N|P67S	vOceania
N|P80R	P.1
N|S206F	vOceania
ORF1A|I4205V	B.1.429
ORF1A|L3458V	P.2
ORF1A|L3930F	P.2
ORF1B|D1183Y	B.1.429
ORF3A|G172V	vOceania
ORF3A|S171L	vAfrica
ORF3A|T223I	v3
ORF8|R52I	v2
ORF8|Y73C	v2
S|D138Y	P.1
S|H655Y	P.1
S|K417T	P.1
S|L452R	B.1.429
S|N439K	B.1.258_DELTA
S|N501T	vOceania
S|P26S	P.1
S|R190S	P.1
S|R246I	B.1.351
S|S13I	B.1.429

S|S477N	v1
S|T1027I	P.1
S|T20N	P.1
S|V1176F	P.2
S|W152C	B.1.429

List 2

Variant_Mutation_1	Variant_Mutation_2	Variant_ID
S|N501Y	S|D614G	P.1,B.1.1.7,B.1.351,B.1.1.7_E484K
S|N501Y	S|E484K	P.1,B.1.351,B.1.1.7_E484K
S|N501Y	S|L18F	P.1,B.1.351
S|N501Y	S|K417T	P.1
S|N501Y	S|T20N	P.1
S|N501Y	S|P26S	P.1
S|N501Y	S|D138Y	P.1
S|N501Y	S|R190S	P.1
S|N501Y	S|H655Y	P.1
S|N501Y	S|T1027I	P.1
S|N501Y	N|P80R	P.1
S|N501Y	S|H69-	B.1.1.7,B.1.1.7_E484K
S|N501Y	S|V70-	B.1.1.7,B.1.1.7_E484K
S|N501Y	S|Y144-	B.1.1.7,B.1.1.7_E484K
S|N501Y	S|A570D	B.1.1.7,B.1.1.7_E484K
S|N501Y	S|P681H	B.1.1.7,B.1.1.7_E484K
S|N501Y	S|T716I	B.1.1.7,B.1.1.7_E484K
S|N501Y	S|S982A	B.1.1.7,B.1.1.7_E484K
S|N501Y	S|D1118H	B.1.1.7,B.1.1.7_E484K
S|N501Y	ORF8|Q27*	B.1.1.7,B.1.1.7_E484K
S|N501Y	N|D3L	B.1.1.7,B.1.1.7_E484K

S|N501Y	N|S235F	B.1.1.7,B.1.1.7_E484K
S|N501Y	S|K417N	B.1.351
S|N501Y	S|D80A	B.1.351
S|N501Y	S|D215G	B.1.351
S|N501Y	S|R246I	B.1.351
S|N501Y	S|A701V	B.1.351
S|N501Y	N|T205I	B.1.351
S|N501Y	DELETION_S_242-245	B.1.351
S|L452R	S|S13I	B.1.429
S|L452R	S|W152C	B.1.429
S|L452R	S|L452R	B.1.429
S|E484K	S|D614G	P.2
S|E484K	S|V1176F	P.2
S|E484K	N|A119S	P.2
S|E484K	N|M234I	P.2
S|H69-	S|N439K	B.1.258_DELTA
S|V70-	S|N439K	B.1.258_DELTA

List 3

Variant_Mutation_1	Epistatically_Linked_Mutation	Variant_ID
N|M234I	N|A376T	P.2,v1
S|N501Y	N|S235F	B.1.1.7,B.1.1.7_E484K,B.1.351,P.1,v2,vAfrica
S|L18F	ORF7B|S5L	B.1.351,P.1,vAfrica
S|P681H	N|G204R	B.1.1.7,B.1.1.7_E484K,v2
S|P681H	N|R203K	B.1.1.7,B.1.1.7_E484K,v2
ORF8|Q27*	N|G204R	B.1.1.7,B.1.1.7_E484K
S|V1176F	N|G204R	P.2
ORF8|Q27*	N|R203K	B.1.1.7,B.1.1.7_E484K
S|V1176F	N|R203K	P.2

S|L18F	ORF8|A65V	B.1.351,P.1,vAfrica
S|N501Y	N|G204R	B.1.1.7,B.1.1.7_E484K,B.1.351,P.1,v2,vAfrica
S|N501Y	N|R203K	B.1.1.7,B.1.1.7_E484K,B.1.351,P.1,v2,vAfrica
N|M234I	ORF3A|Q57H	P.2,v1
N|M234I	S|S477N	P.2,v1
N|T205I	ORF3A|Q57H	B.1.351,vAfrica
N|M234I	ORF7A|T14I	P.2,v1
N|M234I	ORF3A|Q57H	P.2,v1
N|M234I	ORF8|S84L	P.2,v1

Table S5

ORF	FirstNuc	SecondNuc	#Variants
ORF1ab	12621	12747	1043
ORF1ab	13342	13460	1255
ORF1ab	14010	14136	1277
ORF1ab	15431	15530	1897
ORF1ab	18778	18909	8494
E	26269	26381	1640
N	28287	28358	3944
N	28681	28752	4026
N	28881	28979	61834
N	29125	29282	6332